A Review of Laser Powder Bed Fusion Additive Manufacturing of Aluminium Alloys: Microstructure and Properties

H. R. Kotadia[1], G. Gibbons[1], A. Das[2], P. D. Howes[3]

[1]WMG (Warwick Manufacturing Group), University of Warwick, Coventry, CV4 7AL, UK

[2]College of Engineering, Swansea University Bay Campus, Fabian Way, Swansea, SA1 8EN, UK

[3]School of Engineering, London South Bank University, 103 Borough Road, London SE1 0AA, UK

Abstract: Additive manufacturing (AM) of metallic alloys for structural and functional applications has attracted significant interest in the last two decades as it brings a step change in the philosophy of design and manufacturing. The ability to design and fabricate complex geometries not amenable to conventional manufacturing, and the potential to reduce component weight without compromising performance, is particularly attractive for aerospace and automotive applications. This has culminated in rapid progress in AM with Ti- and Ni-based alloys. In contrast, the development of AM with Al-alloys has been slow, despite their widespread adoption in industry owing to an excellent combination of low density and high strength-to-weight ratio. Research to date has focused on castable and weldable AlSiMg-based alloys (which are less desirable for demanding structural applications), as well as on the development of new AM-specific AlMgSc alloys (based on 5xxx series). However, high strength wrought Al-alloys have typically been unsuitable for AM due to their unfavourable microstructural characteristics under rapid directional solidification conditions. Nevertheless, recent research has shown that there is promise in overcoming the associated challenges. Herein, we present a review of the current status of AM with Al-alloys. We primarily focus on the microstructural characteristics, and on exploring how these influence mechanical properties. The current metallurgical understanding of microstructure and defect formation in Al-alloys during AM is discussed, along with recent promising research exploring various microstructural modification methodologies. Finally, the remaining challenges in the development of AM with high-strength Al-alloys are discussed.

Keywords: Aluminium; Additive Manufacturing; Powder Bed Fusion (PBF); Solidification; Microstructure; Mechanical properties.

Please cite this article as:

H.R. Kotadia, G. Gibbons, A. Das and P.D. Howes, AReview of Laser Powder Bed Fusion Additive Manufacturing of Aluminium Alloys: Microstructure and Properties, Additive Manufacturing, Volume 46, October 2021, 102155; https://doi.org/10.1016/j.addma.2021.102155

1 Introduction

After over twenty years of development, metal additive manufacturing (AM) has become one of the most exciting and rapidly developing methodologies in advanced manufacturing [1]. It is receiving significant attention in metal manufacturing as it overcomes many limitations that were once considered inherent in mass production, for example the production of complex geometries, easily customisable structures, and significant weight saving while maintaining strength and structural integrity [1-4]. The approach is inherently different to the more traditional processing methods (e.g. casting, rolling, extrusion and machining), as these formative and subtractive approaches are replaced with layer-by-layer fabrication, literally the 'printing' of metal, pixel by pixel. This allows unprecedented freedom in the manufacturing of complex structures, using unconventional materials with no additional tooling to achieve extremely high precision and control [5]. A further impressive advantage of AM is a significantly reduced manufacturing lead-time, as new designs/components will have a shorter time to market, and customer demand will be met more quickly, all with much reduced material waste during the manufacture [5-7]. Such advantages do, however, need to be balanced against some inherent disadvantages, including the current high cost of AM systems, potentially long build times, and complex and expensive powder feedstocks.

A range of important metal alloy systems have been used for AM, mainly by powder bed fusion (PBF), which uses an intense heat source (e.g. laser, electron beam, plasma-electric arc) to yield highly selective melting of forming layers [4, 5, 8]. A majority of metal AM research focuses on high temperature alloys, such as Ti-6Al-4V [9-12], TiAl [13, 14], Inconel 625/718 [15-20] and Cobalt Chromium (CoCr) [21, 22], and indeed these have found application in real-world AM practices. In the last five years, a significant amount of research has been carried out on various grades of steel, including stainless steel (austenitic, maraging and precipitation hardened), low carbon steel, and tool steels [2, 23, 24]. In comparison, exploration of AM capability of Al-alloys has been limited [25]. Importantly, "printable" Al-alloys are still near eutectic Al-Si based alloys (e.g. AlSi7Mg, AlSi10Mg and AlSi12Mg), because of their short freezing range [1, 26].

For widespread industrial adoption of AM, it is essential that manufactured objects provide the desired properties for the intended use, whilst keeping cost-of-production competitive. It is, therefore, necessary to improve the fundamental understanding of AM metal processing through careful investigation of multiple chemical and physical phenomena across various time and length scales (**Figure 1**) [27]. An important consideration is that, when a laser beam irradiates a metal powder, all the four states of matter (i.e. solid, liquid, gas, plasma) are present simultaneously, giving rise to material interactions that are unseen in conventional processing. Further, the use of rapid thermal cycling gives rise to sharp thermal gradients and possible metastable physical and chemical states that can generate undesirable metallurgical defects [28]. This is a key problem in AM of Al, and has become a barrier to widespread adoption, along with the currently limited number of suitable alloys.

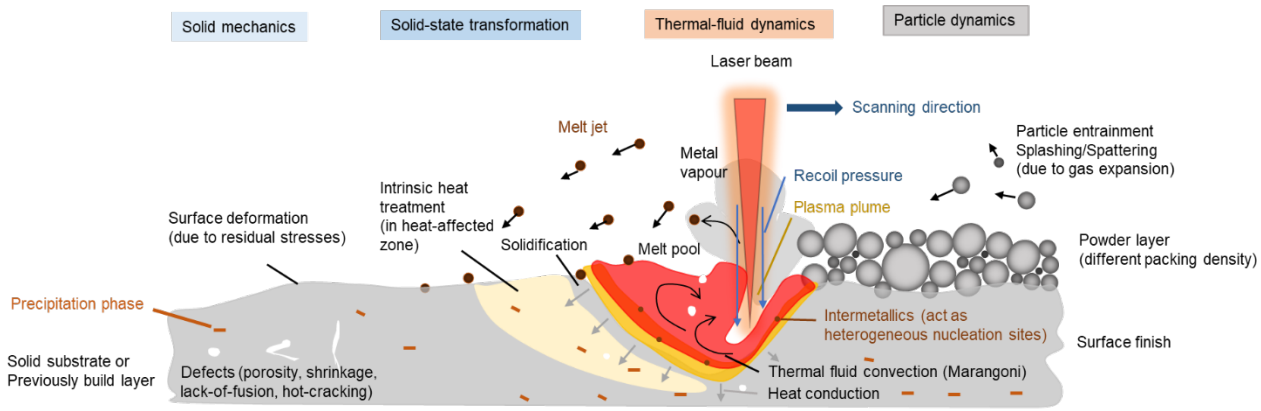

Figure 1. Schematic illustration of the Laser-Powder Bed Fusion (L-PBF) process and associated multiple physical and chemical phenomena, showing the various phenomena influenced by laser-powder interaction, solidification and solid-state transformation. Adapted from Ref. [27].

This review aims to provide an overview of the various different Al-alloys in use today in Laser PBF (L-PBF) based AM, highlighting the progress made in the last five years. The main focus is microstructural evolution with respect to alloy chemistry, in particular the effect of rapid solidification in comparison with conventional manufacturing, and the resultant mechanical properties. We do not cover the various AM processing methods and parameters required to achieve higher relative density in detail; such information can be found in other recent reviews [1-4, 25, 26]. Instead, the influence of process parameters on the microstructure, wherever relevant, is discussed. It has been decided to restrict the scope to the L-PBF process. However, electron beam melting (EBM) is entirely capable of processing Al, and the reader is encouraged

to seek information available in other reviews. Some of the sections are kept brief, for two reasons. First, when an already detailed review has been published covering that area, and second, when no clear conclusion could be drawn from the existing literature. The discussion is split into the following sections: (i) cast Al-Si alloys, (iii) wrought Al-Alloys covering AM specific alloy, (iii) primary-Al grain refining, and (iv) powder feedstock.

2 Aluminium alloys and their applications

Al is the second most widely used structural metal after steel, globally, with over 67 Mt produced in 2019 [29]. The use of Al-alloys continues to grow at around ca. 6% per annum [30], mainly due to its low density (three times lighter than steel), high corrosion resistance, and excellent combination of physical and mechanical properties [31]. The application of light alloys, predominantly Al-alloys, is projected to double within the transport sector in the next decade. The ASTM standard classification of Al-alloys splits them into two groups—cast and wrought—which are designated with a four-digit numerical code (**Table 1**) [31]. Currently, about 80% of Al-alloy used in structural applications are wrought products [32], produced either by rolling, extrusion or forging. Cast Al-alloys are produced through various casting techniques, such as sand casting, gravity casting, high-pressure die casting (HPDC), and investment casting, depending on the alloys, component features (shape, size, quality) and cost considerations.

For structural applications, strengthening is essential for pure Al as it is too weak in pure form. In contrast to steel, Al does not exhibit an allotropic phase transformation, which limits strengthening via phase transformation. Cast Al-alloys mainly contain Si, with Cu and Mg as minor alloying elements. The addition of Si forms a classical eutectic system, improving castability and fluidity [31, 33]. The phase diagram (**Figure 2 (a)**) shows a eutectic point at ca.12.7 wt.% Si and 579 °C and the different microstructure formed due to a variation in alloy composition across the eutectic point is illustrated in **Figure 2 (c)**. Al-Si based alloys used in AM are often multicomponent, such as the popular AlSi10Mg alloy. Thermodynamic software can provide valuable information on the phase evolution and solidification parameters in such systems for assessing suitability of the alloy for AM as well as selection of process parameters. For example, ThermoCalc generated phase fraction data for AlSi10Mg presented in **Figure 2 (b)** not only shows the relative fraction of phases formed in the alloy, but also indicates a freezing point of 593 °C for Al solidification, eutectic temperature of 574 °C and a freezing range of 31 °C. The microstructure of cast Al-Si alloys can be refined through chemical

inoculation, for example with NiB [34], to refine the primary Al grain size, P to refine primary-Si [35], and Sr to refine eutectic Si [36-38]. Microstructural refinement can also be achieved by the application of physical force such as ultrasonication [39-43], shearing [44-46], electromagnetic fields [47-49], and/or by modifying processing conditions [50, 51], such as cooling rate. Further, added elements such as Cu and Mg serves to improve mechanical properties through precipitation strengthening (using dispersion of Al_2Cu, $Al_5Mg_8Cu_{26}$) [31, 33]. Of the world production of Al, ca. 20% is used for cast products with a wide range of applications, including automotive powertrains.

Wrought Al-alloys are separated into two distinct classes: heat treatable (2xxx, 6xxx, 7xxx) and non-heat treatable (1xxx, 3xxx, 5xxx). Non-heat-treatable alloys mainly achieve strength through cold work (strain hardening). For example, 5xxx AlMg(Mn) alloys have been shown to exhibit a decent combination of strength and formability. To achieve the desired mechanical properties, various alloying elements are added, followed by complex thermo-mechanical processing routes. Alloying elements such as Cu, Mg, Si, Zn, Li, Sc are added into Al to allow Al_2Cu, Al_2CuLi, $Mg_5Si_4Al_2$, Mg_2Si, $MgZn_2$, Al_3Sc intermetallics to precipitate through suitable heat treatment [31, 33]. Further, some transition elements, e.g., Cr, Mn or Zr, can be added to form $Al_{12}Mg_2Cr$, $Al_{20}CuMn_3$, $Al_{12}Mn_3Si$ and Al_3Zr dispersoid particles to allow control of grain structure during thermo-mechanical processing [52]. The coherency, volume fraction and distribution of these particles plays a key role in strengthening. Heat treatable 2xxx, 6xxx and 7xxx alloys are used in aerospace and automotive applications due to their improved strength after heat treatment along with excellent corrosion resistance [31, 53]. It is worth mentioning that AM components experience completely different heating and cooling conditions to conventional manufacturing routes, therefore, the sequence and rate of precipitation phase formation can be very different. Jägle et al. [54] demonstrated that some precipitation phase can form during production of the powder feedstock and during the printing (due to repetitive heating and cooling). In addition, due to rapid solidification in AM, solute trapping is common. This also contributes precipitation strengthening during stress relieving treatment. Therefore, it is important to understand the entire AM cycle and control the thermal profile to achieve desirable precipitation phases and properties.

Table 1. Cast and wrought alloy designation (alloy compositions are expressed in wt.%).

Cast Aluminium Designation	**Wrought Aluminium Designation**	**Applications**

1xx.x	Al (99% minimum or greater)	1xxx	Al (99% minimum or greater) – H	Electrical and chemical industries
2xx.x	Al-Cu (4% to 4.6%)	2xxx	Al-Cu (2.2% to 6.8%) – T	High-strength applications, e.g. aircraft
3xx.x	Al-Si (5% to 17%) with Cu or Mg	3xxx	Al-Mn (0.3% to 1.5%) – H	Architectural and general-purpose applications
4xx.x	Al-Si (5% to 12%)	4xxx	Al-Si (3.6% to 13.5%)-Cu (0.1% to 4.7%)- Mg (0.05% to 1.3%) – H/T	Welding and brazing consumables
5xx.x	Al-Mg (5% to 12%)	5xxx	Al-Mg (0.5% to 5.5%) – H	Rolled products: automotive trim, boat hulls, architectural components
6xx.x	Unused series	6xxx	Al-Mg (0.35% to 1.5%)-Si (0.2% to 1.8%) – T	Structural applications e.g. body-in-white
7xx.x	Al-Zn (6.2% to 7.5%)	7xxx	Al-Zn (0.8% to 8.2%)-Mg (0.1% to 3.4%)-Cu (0.05% to 2.6%) – T	High-strength application, i.e. aircraft structures
8xx.x	Al-Sn	8xxx	Al with other elements like Li, Fe – H/T	
9xx.x	Al with Other elements	9xxx	Unused series	

H: work hardening (non-heat-treatable); T: heat-treatable.

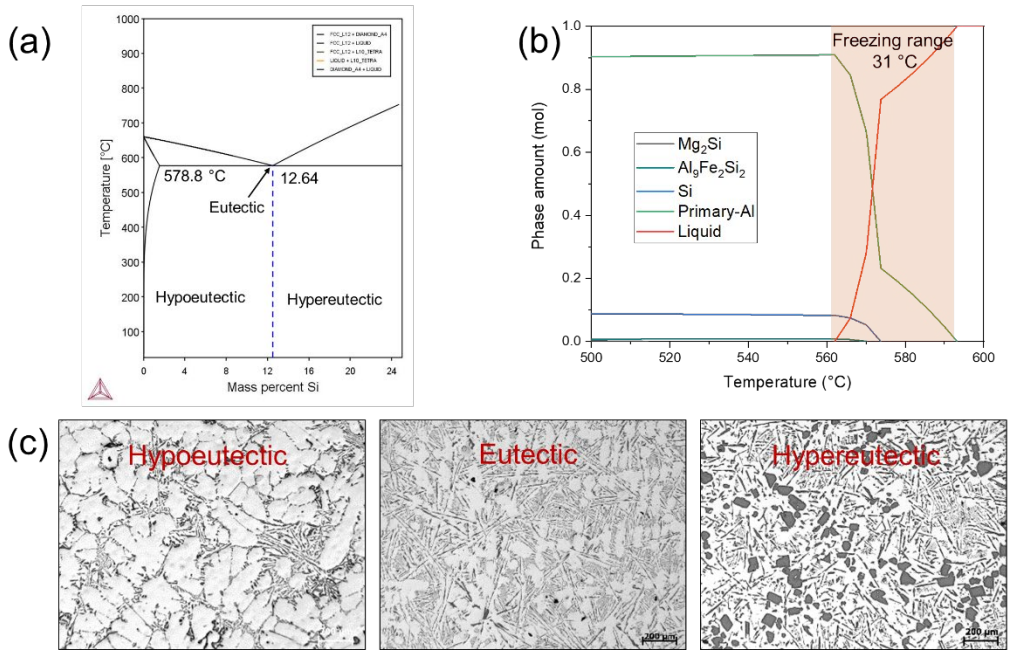

Figure 2. (a) Al-Si binary phase diagram, (b) Thermo Calc generated phase development in AlSi10Mg alloy (which have smaller freezing ranges compared to the wrought Al-alloys, Figure 11), and (c) three different types of microstructure that form in the Al-Si system, as labelled (where white and dark grey phases represent primary-Al, and Si, respectively).

2.1 **AM of Al-alloys**

Processing with AM is inherently different to conventional casting, with significant advantages gained through reduced manufacturing steps and much-reduced waste [5]. The basic process of PBF AM requires the application of a laser to melt and consolidate powder feedstock in layers, gradually building up a 3D structure. Coupled with computer-aided-design (CAD), this approach is extremely powerful, and can achieve structural and geometric complexity that is unthinkable with traditional processing (e.g. complex foams, hollow structures, lattices), ultimately allowing highly effective use of material whilst obtaining excellent strength-to-weight ratio [55]. Lattice structures can be used for further weight saving, to reduced vibration and noise [56]. Further, components can be fabricated with a gradually altering material composition and organisation within a single structure, for example to achieve site-specific properties and 'multifunctionality', balancing mechanical, thermal, magnetic and energy absorbing properties in a way that is otherwise inaccessible.

Rapid solidification of metal alloys may lead to unique structural and mechanical properties, unachievable through conventional solidification [57, 58]. However, conventional casting does not permit high cooling rates through the entire cast, limiting this method to small or thin parts

(e.g. filaments, ribbons, flakes). In contrast, PBF in AM exhibits significant advantages, where laser heating is applied to only small volumes of material at a time. Coupled with short laser irradiation times, very high heating and cooling rates can be achieved (10^3–10^8 K/s) [59, 60]. This results in very different processing conditions, and subsequent metallurgical response, compared to conventional casting processes.

One of the most important features under PBF AM is the rapid heating and cooling experienced. The effect of rapid solidification on the Al-alloy microstructure can be delineated along three lines [61]. First, *constitutional changes* arise due to a high degree of undercooling during rapid solidification. In more extreme conditions this can result in partitionless (i.e. segregation free) solidification. Second, *individual phase refinements* occur, where the degree of microstructural refinement is closely linked to the velocity of the solidification interface [62, 63]. Third, *formation of metastable phases* (e.g. Al_6Fe in Al-Fe [64], and Al_6Mn in Al-Mn [65]), including amorphous structures formed by some rapidly solidifying alloys, and quasicrystalline phases that may form depending on the alloying addition even at modest cooling rates. The intrinsic microstructural features typically seen in aluminium alloys after rapid solidification include refined microstructural features such as reduced dendritic arm spacing, a decrease in segregation patterns, solid solubility extensions of alloying elements in primary-Al (solute trapping effect), metastable crystalline phase formation, amorphous structures, and quasicrystals [61].

It is understood that grain structure has a major influence on material properties. Grain size greatly influences mechanical strength, as elucidated by the Hall–Petch relationship [66, 67] ($\sigma_y = \sigma_0 + k/\sqrt{d}$), which shows that the yield strength (σ_y) of polycrystals is inversely proportional to the square-root of grain size (d), where σ_0 is the frictional stress (which is independent of grain size), and k is a material constant. High cooling rates during manufacturing makes PBF an excellent candidate for creating fine microstructures, which holds great promise to improve mechanical properties of components compared to manufacturing based on conventional casting methods. The grain size of L-PBF of Al alloys (~≥50μm) typically falls within the original Hall–Petch relation leading to strength enhancement. However, many grains have a propensity to columnar rather than equiaxed morphology in the building direction. Therefore, mechanical properties could be anisotropic and it is also important for researchers to be specific about grain dimensions used for analysis. Alloy strengthening can also be improved and tailored by controlling eutectic, precipitation, dispersoids, intermetallic and metastable phases [33].

The use of Al powders in PBF is especially promising due to the high thermal conductivity and low specific gravity of Al, which should allow the fabrication of lightweight and heat-controllable builds (e.g. heat sinks and heat exchangers). However, most of the current "printable" Al alloys are still the relatively low strength near-eutectic AlSiMg-based alloys rather than those based on high-strength wrought alloys [26, 68]. Another class of printable Al is based on 2xxx (Al-Cu) with higher Ti, such as A20X™ alloy (Al-4.5Cu-0.3Mg-0.7Ag-3.5Ti) developed by Aeromet, 5xxx (Al-Mg) with Sc and Zr such as the Scalmalloy® (Al-4.5Mg-0.6Sc-0.5Mn-0.3 Zr) developed by Airbus Group Innovations [56, 69], and 7xxx (Al-Zn) with higher Zr such as Al-7A77 alloy (Al-5.5Zn-1.5Cu-2.5Mg-1.5Zr) developed by HRL laboratory, which was designed specifically for PBF processing.

To date, research activity in AM with Al alloys has been restricted versus other alloys. There are a number of factors that complicate the process, including surface oxide formation in the powders, poor powder flowability, low absorptivity of Al alloys at the wavelengths of some common laser sources, and high material thermal conductivity [70]. In particular, the combination of high thermal conductivity and low absorptivity requires the application of very high energies to achieve powder melting. However, this can yield uneven vaporisation of alloys where the high vapour pressure alloying elements (e.g. Zn and Mg) preferentially vaporise [2, 26]. This then leads to heterogeneity within the final build.

Table 2 shows the chemical compositions of the Al-alloys most widely used in AM, with their descriptive name. Most of the Sc-containing alloys are not commercially available, and their powders are only available from limited suppliers. Further, typical commercial high-strength wrought alloys (with tensile strengths up to 500 MPa with good ductility over 10% after heat-treatment [31]) exhibit poor PBF processability because of hot cracking [68]. Consequently, research into new ways to enhance PBF-processability of these alloys has high significance. **Figure 3** summarises the overall tensile properties of conventional Al-alloys and currently tested alloys after L-PBF. This clearly shows that Al-alloys manufactured through L-PBF can achieve a similar tensile strength, but with reduced ductility, a point that will be discussed in detail in a subsequent section.

Table 2 List of selected Al-alloys used in L-PBF and their tensile properties in simple geometry (rectangular) builds. All studies were carried out using locally optimised processing conditions, but not necessarily fully optimised. Further, most recorded an Archimedes density above 99 %. Note that we have omitted literature on wrought alloys that has not exhibited acceptable properties due to defects. For given property ranges, we present only select references.

	Composition	Conditions	AM-processed tensile properties			Ref.
			UTS* (MPa)	YS* (MPa)	Elongation to break (%)	
Cast Alloys	A356 (Al-7Si-0.6Mg)	L-PBF	368	275	9	[71]
		T2	226	150	12.8	[71]
	AlSi10Mg, (Al-10Si-0.32Mg-0.03Cu)	L-PBF	315–446	209–270	1–8	[72-74]
		L-PBF + T6	140–358	100–2041	10–25	[72-74]
	AlSi12 (Al-12Si-Fe)	L-PBF	350–425	100–260	2.5–4.5	[75-77]
		L-PBF + Solution heat treatment	150	95	15	[75-77]
	Al-20Si	L-PBF	506	374	1.6	[78]
		L-PBF + 400 °C for 6 h	252	162	8.7	[78]
Wrought Alloys	2xxx (2024: Al-4.35Cu-1.50Mg-0.25Fe-0.60Mn-0.08Ti-0.05Cr)	L-PBF with Grain refiner + T6	432	286	10	[79]
	2xxx (A20X: Al-4.5Cu-0.3Mg-0.7Ag-3.5Ti)	L-PBF + 530 °C for 1 h + 160 °C 3 h	425	375	10	[80]
	5xxx (Scalmalloy®: Al-4.5Mg-0.6Sc-0.5Mn-0.3 Zr)	L-PBF	431	410	13	[81]
		L-PBF + Aging at 300 °C, 5 h	570	500	4.3	[81]
	6xxx (6061: Al-0.9Mg-0.7Si-0.3Cu-0.3Fe-0.1Ti)	L-PBF (with heated build plate at 500 °C)	318	290	5.4	[82]
	7xxx (7075: Al-5.5Zn-2.5Mg-1.6Cu-0.4Si-0.3Fe-0.2Cu-0.2Ti)	L-PBF with Grain refiner + T6	383–417	325–373	3.8–5.4	[73]
	7xxx (Al-7A77: Al-5.5Zn-1.5Cu-2.5Mg-1.5Zr)	L-PBF + T6	550	525	10	[83]

* UTS: Ultimate tensile strength; YS: Yield strength at 0.2% offset.

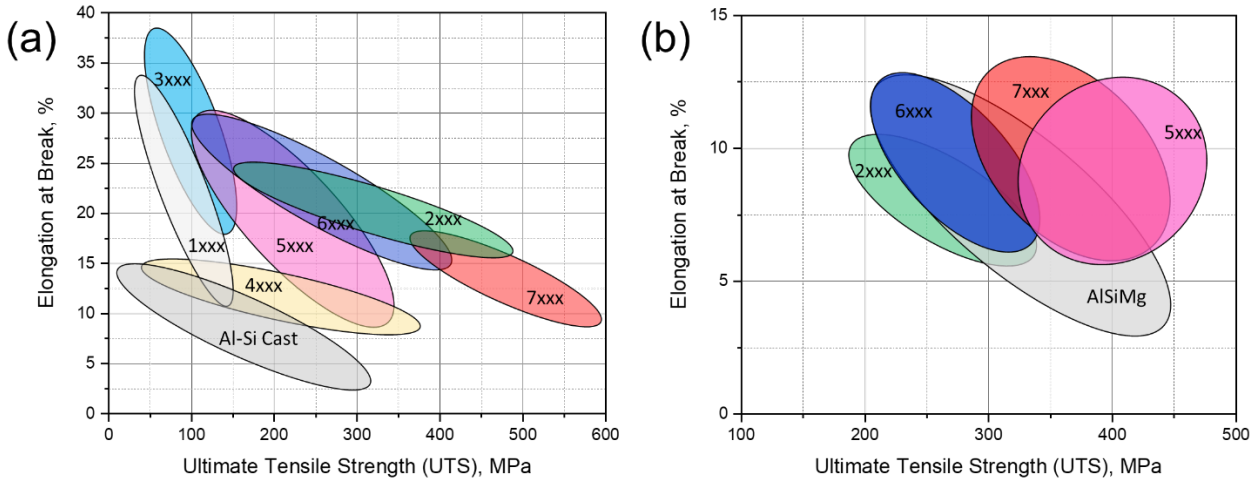

Figure 3. Tensile properties of (a) conventional Al-alloys [31] and (b) selected L-PBF Al alloys.

3 Al-Si alloy in AM

Near-eutectic Al-Si alloys possess outstanding fluidity, high thermal conductivity, low coefficient of thermal expansion (CTE) and excellent castability, therefore the majority of Al-alloys used for PBF are hypoeutectic Al-Si (7–12 wt.%)-Mg (>1 wt.%) alloys. A small number of publications [77, 78, 84] have used hyper-eutectic alloys with higher Si content, made by mixing Al powder with Si.

3.1 Microstructure of L-PBF-fabricated Al-Si alloys

3.1.1 *Hypoeutectic Al-Si alloy*

Microstructural evolution during solidification is a critical factor in determining the final mechanical properties of L-PBF processed parts. The main microstructural features present in L-PBF produced hypoeutectic Al-Si alloys are primary-Al grains and the eutectic Si phase. A common primary-Al grain morphology observed after L-PBF is the epitaxial columnar grain (**Figure 4 (a)**) [85, 86]. Such columnar grains, which are aligned parallel to the build (vertical) direction, are responsible for the anisotropic mechanical properties observed in AM-made metal parts. Epitaxial columnar grains grow due to partial melting of the previously solidified layer during material deposition and propagate through many successive build layers. This induces a sufficient thermal gradient in the melt pool, along with the release of latent heat preventing fresh nucleation ahead of the solidification front. Electron backscatter diffraction

(EBSD) studies have revealed that these columnar grains exhibit <001> fibre texture [85, 86]. Long columnar grains formed due to directional heat transfer under a steep temperature gradient (arising due to high heating and cooling rates), with the boundaries between them enriched with eutectic liquid during solidification. Wu et al. [85] noted that these long cells forming within columnar grains do not alter their orientation during growth as Al within the eutectic deposits and grows on the existing Al cells (**Figure 4 (e) and (f)**). In their work, the reported columnar grain sizes were a few hundred μm, with cell sizes of a few μm. They showed that an epitaxial relationship exists between the eutectic Si and Al (described as (111)Si||(200)Al). In conventional casting, where cooling rates are less than 10 K/s, Si particles are seen to grow as needle or plate-like structures within the dendritic microstructure of the Al grains (with typical <110> growth direction) (**Figure 2 (c)**). In contrast, under the high cooling rates (10^3–10^8 K/s) during L-PBF processing, these alloys form an ultrafine eutectic Si microstructure (**Figure 4 (c) to (d)**), ca. 10–100 nm in size around the cell and grain boundaries (**Figure 4 (g) to (h))**. The extremely fine cellular microstructure, with ultrafine eutectic microstructure, leads to significant enhancement in the mechanical behaviour of L-PBF processed samples.

Optimised processing parameters should be employed during L-PBF to build components with a fine microstructure and desirable mechanical properties [72, 87]. The eutectic Si microstructure in PBF is controlled by various factors, including kinetics, thermodynamics (i.e. the wettability) and the local concentration of Al and Si atoms. In PBF, due to the moving heating source, thermal gradients and growth rates vary within the melt pool, leading to differences in microstructure and texture within the build [88]. Many researchers [86, 88, 89] have explored this, attempting to alter the alloy microstructure by modifying the melt-pool by controlling processing conditions. For example, Thijs et al. [88] hypothesised a solute redistribution effect that is distinctly different from that observed in conventional casting. They observed that Si solubility dramatically increased in the solid-Al because of rapid cooling. Hence, a supersaturated Al solid solution, possessing a fine cellular-dendritic structure, forms along with fibrous eutectic Si at the cell boundaries. The solute concentration of Si in the liquid Al is affected by the rates of cooling and diffusion, which can be controlled by several processing parameters, including laser power and scanning speed. Furthermore, the short irradiation time of the material by the laser, and the formation of liquid oscillations or capillary waves, will also tend to generate a heterogeneous microstructure in the melt pool [90]. Accordingly, various researchers have studied such effects by implementing different scanning strategies to alter the grain structure and improve L-PBF build quality [88, 91, 92].

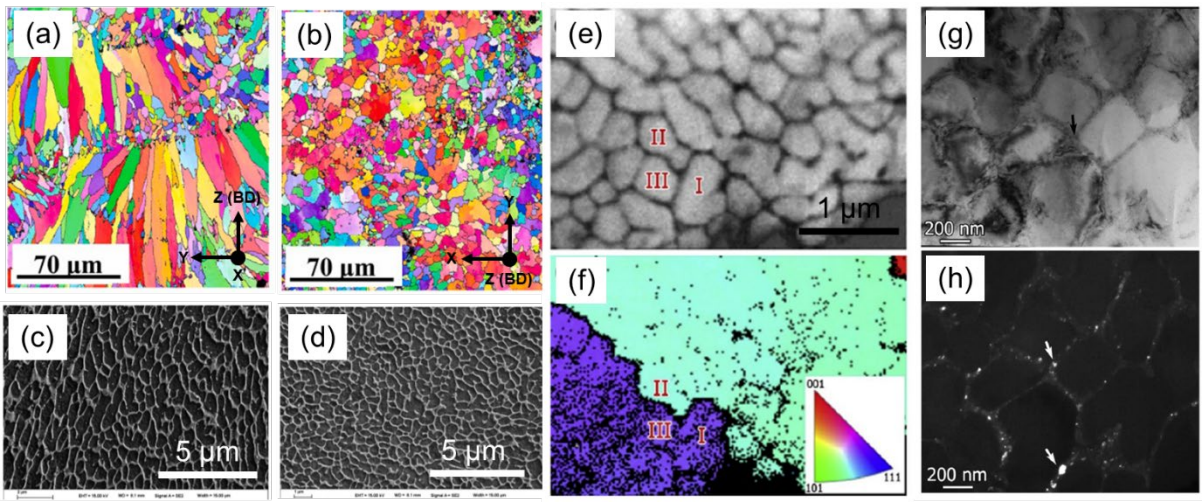

Figure 4. Hypereutectic AlSiMg alloy microstructural features. EBSD image showing (a) primary-Al columnar grain <001> fibre texture in build direction (ZY), (b) primary-Al columnar grain structure in horizontal (XY) direction (reprinted from Ref. [93]). SEM images of (c) ZY and (d) XY, showing a fine eutectic structure (reprinted from Ref. [94]). High magnification micrographs, showing (e) a band contrast image and (f) an orientation map, show a similar orientation of cell structures within primary-Al grain. TEM image in (g) and (h) showing fine eutectic Si within the cells, reprint from Ref. [85].

3.1.2 ***Hypereutectic Al-Si alloy***

The microstructure of hypereutectic Al-Si alloys contains primary Si particles and a eutectic-Si needle embedded in primary-Al matrix, with the primary Si particles yielding high strength and wear resistance. In conventional casting, faceted and 'blocky' primary-Si particles form (**Figure 2 (c)**) leading to low ductility, poor wear performance and low machinability, which greatly restricts their application. These limitations can be addressed by refining primary-Si particles and distributing them uniformly within the Al matrix [41]. In AM, the size of the primary-Si particles is usually < 1 µm [78, 84, 95], compared to 25–50 µm in conventional casting [41], for alloy containing up to 20 wt.% Si. Kang et al. [84] showed that in very high Si content Al-50Si alloy, the internal melt pool (close to the laser source) gradually solidified with a lower Si content, whereas the external melt pool produced primary-Si phase with a smaller size due to its higher cooling rate (**Figure 5**). This is due to the primary-Si phase nucleating from the liquid metal being compelled by the fluid flow (Marangoni convection) to solidify in the external melt pool, which is at a lower temperature during L-PBF. Such microsegregation within the build has a substantial effect on the melt pool temperature and size, which is ultimately a function of the energy input [84]. Furthermore, the scanning speed and other processing parameters significantly influence the hypereutectic microstructure,

where higher cooling rates during L-PBF result in a displacement of phases, and hypereutectic alloy may form a microstructure resembling hypoeutectic or eutectic alloys [77].

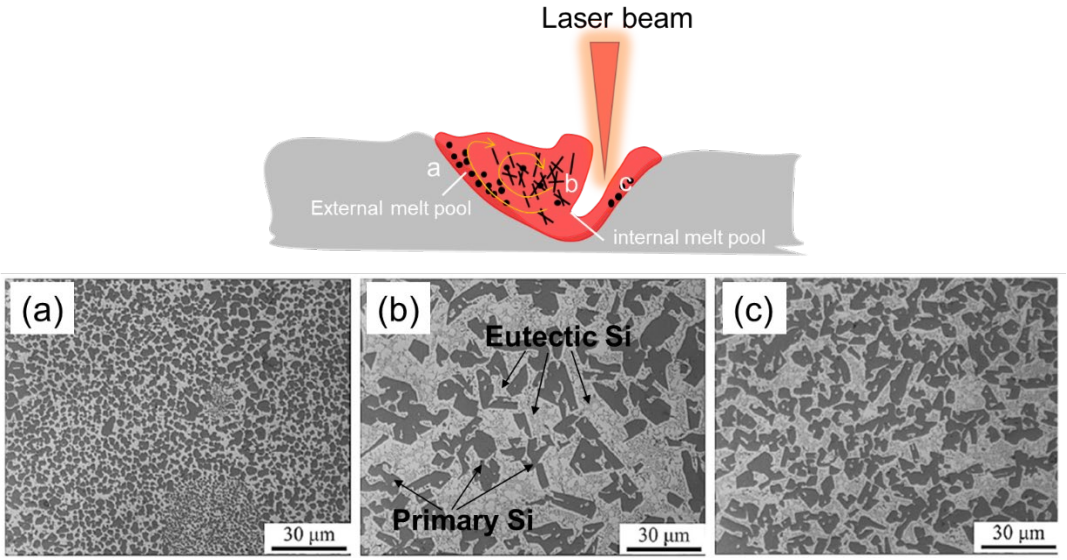

Figure 5. L-PBF processed hypereutectic Al-50Si alloy. The melt pool, and primary-Si and eutectic Si distribution within it. Adapted from Ref. [84] with permission from Elsevier.

The microstructure formed during L-PBF are different between hypo and hyper-eutectic Al-Si alloys. This is mainly due to fraction of phases and differences in primary phase solidification. Primary alpha-Al is the predominant phase in the hypo-eutectic alloys and solidifies with epitaxial and columnar grain structure due to the directional growth under the strong thermal gradient and rapid heat transfer and the minor eutectic is dispersed in the intergranular areas in fine form. On the other hand, considerable eutectic volume exists in the hyper-eutectic alloys where Si nucleates as the primary phase in the form of particulates dispersed in the eutectic liquid. While this avoids columnar grain structure in the hyper-eutectic alloys, the strong thermal gradient and associated fluid flow may lead to inhomogeneous distribution and segregation of the floating Si-particles. Since both the thermal gradient and the rate of cooling affects the solidification condition and fluid flow, laser processing parameters influence the microstructure in both hypo and hyper-eutectic Al-Si alloys despite the difference in their microstructure (and their formation).

3.2 **Defects**

Research has revealed that processing parameters have a dramatic influence on the density of AM Al-Si components because of pore formation [87, 96-98]. This is severely detrimental to the final mechanical properties and fracture resistance of built components. It is known that

processing conditions can be optimised to increase the build density in L-PBF, for example, employing high laser powers and scan speeds combined with low scan spacing. However, much less is known about the effects of material chemistry in the melt pool on final defect formation.

Figure 6 shows various defects observed in AM AlSiMg alloys [26, 99, 100]. The balling phenomenon (**Figure 6 (a)**) is often observed in L-PBF of metallic material, which yields an irregular scan track and poor inter-line bonding. Further, such balling is a significant hindrance during the deposition of fresh powder on to previously melted layers, causing non-uniformity, porosity and sometimes delamination [101]. Therefore, balling severely degrades material properties and part geometry. Irregularly shaped pore defects are a consequence of incomplete fusion and entrapment of gases in these areas. Here, horizontally-aligned defects are commonly associated with an insufficient input energy density and poor fusion between layers, whereas vertically-aligned defects are associated with large distance between adjacent laser scan paths (hatch distances) leading to insufficient overlap between scan tracks [26, 99].

Moisture in the powder stock can give rise to small gas pores (i.e. below 5 μm in diameter) (**Figure 6 (b)**). This is particularly problematic when high energy densities are used. Further, if the moisture reacts with Al, forming Al_2O_3, the hydrogen that is released can be absorbed by the melt. This in turn yields hydrogen-rich pores that increase is size as temperature is increased during the build processes. For example, Weingarten et al. [102] reported that of the pores developed in a L-PBF built A1Si10Mg alloy, 96% were hydrogen. However, it has been shown that pre-drying of powders can inhibit pore enlargement, for example Yang et al. [103] demonstrated that a 16-hour 200 °C pre-drying step in the build chamber yielded a significant improvement in build density.

Large gas pores (> 30 μm in diameter) are related with the keyhole mode of melting, arising from extreme volumetric energy densities, and observed in various locations when alike processing parameters are used for contour (outer edge defining geometry) and core (inner volume of geometry) scans within a layer. The first location is in the contour scan areas, where low heat dissipation into the powder on one side of the melt pool results in excessive heating. The second location is at the core periphery, where acceleration and deceleration of the laser during the change of scan direction leads to an increased local energy density. Pores at these two locations lead to significantly decreased fatigue performance but can typically be alleviated by modulating the energy input during the contour scan and when turning the laser during the core scan. The third typical position of large pores is at the island scan boundaries, when there is excessive boundary overlap [103]. The optimisation of processing parameters for L-PBF of

Al-Si alloys can yield significant control over the formation of these lack of fusion pore (**Figure 6 (c)**) defects, allowing the production of dense components, even without the pre-treatment of feedstocks. Generally, near eutectic Al-Si alloys are not sensitive to solidification cracks or hot-cracking, except when Si content is around 1 wt. % (**Figure 6 (d)**) [104]. These cracks form in PBF samples initially through shrinkage porosity and propagate due to residual stresses generated during the build.

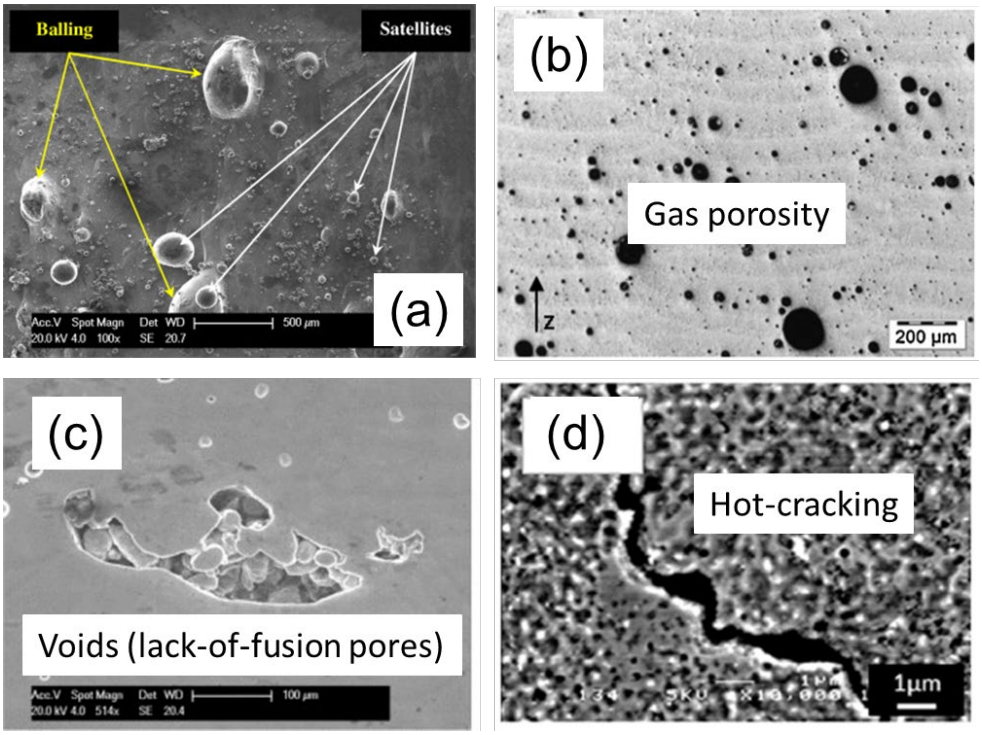

Figure 6. The different types of defects that form during AM of Al-Si alloys by L-PBF: (a) balling, (b) gas pores, (c) voids or lack of fusion pores and (d) hot cracking (Adapted from Refs. [99, 102, 104, 105] with permission from Elsevier). Note that Al-Si exhibits high sensitivity for hot cracks when Si content is around 1 wt. % [104], which is further explained through crack sensitivity graph in Figure 12.

3.3 **Mechanical properties**

*3.3.1 **Effect of microstructure characteristics and processing conditions***

It is well established that Si plays an important role in both material castability and the resultant mechanical properties of Al-Si alloys [33]. In conventionally solidified alloys, the needle or plate-like shapes of the Si phase lead to localised shearing during the early stages of tensile loading and plastic deformation, and quickly to initiation and propagation of cracks, and

fracture [106]. However, in L-PBF, the spherical Si nano-sized phase forming at the eutectic regions and in the cells resists local shearing forces. This results in a suppression of crack initiation and propagation and yields an improvement in ductility and strength. The relevant literature suggests that this enhances tensile properties of AM hypoeutectic Al-Si alloys in comparison with conventionally cast material. Furthermore, these high tensile properties of L-PBF builds are also contributed by the non-equilibrium solubility of Si in the Al matrix, in addition to the microstructural refinement of the eutectic Si particles and primary-Al grains. Similar to the hypoeutectic alloys, the strength of hypereutectic alloys also improves through refining primary-Si and eutectic Si phases.

Furthermore, in contrast to conventional casting, Al-Si L-PBF parts show differences in microstructure in the vertical 'build' direction versus the horizontal, leading to anisotropic characteristics [93]. It is not easy to control such isotropic tensile strengths, and anisotropy of ductility, using post-build treatments [87, 97, 107, 108]. In contrast, although anisotropic properties are seen for Al-Si alloys in L-PBF, it is possible to obtain good tensile properties under different fabrication conditions [109, 110] and most of the literature has noted that tensile strengths of Al-Si in the two directions are essentially the same [26].

It has also been observed that changing the scanning strategy, such as varying hatch style and contour, significantly changes the texture [88] and improves tensile properties, which is mainly attributed to altered crack propagation paths [111]. It is noted that L-PBF samples also possess improved toughness, however, this effect is very sensitive to processing parameters such as build and scan direction.

Most researchers have noted that the fatigue properties of L-PBF samples are worse than those of cast samples. The presence of tensile residual stresses, porosity, and unmelted particles have been found to be the likely reasons for this [112]. Further, it has been observed that fracture occurs most commonly in the heat-affected zone (HAZ) at the melt pool boundary. The size of the HAZ is strongly dependent on the L-PBF processing parameters, which yields a ready way of tuning the thermal gradients in the HAZ and melt pool. Specifically, a steeper gradient reduces the size of the HAZ, which is in theory beneficial as it reduces the chance of fracture. Studies on the effect of different environments, such as Ar, N_2, and He, have concluded that Ar and N_2 produce samples with superior mechanical properties compared to He (especially ductility). This has been explained by the formation of pore clusters [113].

3.3.2 ***Effect of heat treatment***

The tensile properties of AlSiMg alloys can be further improved through solution and aging heat treatment. These alloys have varying amounts of Mg and Cu, apart from the Si, to enhance mechanical properties through precipitation strengthening. Overall, the precipitation mechanism during aging follows the evolution of metastable and stable phases, as studied by Edwards et al [114] and Donlon [115] and others e.g. Ref. [116]. It was found that the precipitation sequence follows: super saturated solid solution (SSSS) → independent clusters of Mg, Si and Cu atoms → GP (Guinier-Preston) zones → needle-shaped β″→ rod-shaped β′ → plate-shaped β.

A large amount of research has been conducted on the heat treatment of various AM Al-Si alloys processed through L-PBF, and on the relationship of between build plate temperatures and the resultant microstructures [107, 117, 118].

The thermal environment is also a key parameter in determining the mechanical properties of L-PBF built sample [119, 120]. For example, Siddique et al. [121, 122] studied the mechanical properties of AlSi12 as a function of build rate, base plate pre-heating and post-build heat treatment. Their result showed that these parameters affect microstructure and improve fatigue performance of parts produced through L-PBF. While Buchbinder et al. [110] found that preheating the base plate led to grain coarsening and decreased hardness, for AlSi10Mg, it was actually beneficial in minimising defects in the final microstructure. A heated build plate also enhances adhesion of the part to the platform and reduces residual and thermal stresses.

Particular emphasis is placed on the Si particle morphology at various conditions, as well as the on the evolution of mechanical properties. The most commonly applied heat treatments to these alloys are ASTM – T4, T5, T6, and T7. The size, shape and distribution of the eutectic Si phase have an important influence on the mechanical properties of Al–Si alloys. **Figure 7** shows a schematic of the microstructural evolution of eutectic Si during the annealing treatment [75]. By increasing annealing temperature or time, eutectic Si grows and total number density decreases. It has been shown that spherical Si particles (diameter < 100 nm) form at Al grain boundaries because of the extreme cooling rates encountered during L-PBF [85]. It is thought that this microstructure explains the high tensile ductility (up to 25% for the AlSiMg alloy), but that it arises at the expense of yield and ultimate tensile strength. Nevertheless, the microstructure of Al-Si alloys can be tailored by altering heat treatment procedures.

In addition, compared to conventional casting, the rapid cooling rate experienced by L-PBF-processed samples can result in a higher solute supersaturation than the equilibrium

microstructure, which is known as solute trapping. Rao et al. [117] studied AlSi7Mg0.6 alloy processed through L-PBF, where the initial Si concentration in the Al matrix was 5.4 wt.%, and reduced to 0.5 wt.% after a 1 hour solution treatment at 535 °C. Therefore, the high supersaturation of Si and Mg in Al, achieved in L-PBF processed alloys, may allow direct artificial aging. Further, the level of supersaturation is significantly higher than what can be obtained during conventional solution treatment. This can yield higher peak hardness in comparison with that achievable by solution heat-treated L-PBF and casting (**Figure 8**), therefore we can conclude that standard precipitation strengthening heat treatment is likely not optimal for L-PBF alloys. In fact, a majority of desired microstructures are obtainable through the use of lower temperatures and shorter solution heat treatments than those recommended for ASM T6 [31] (e.g. less than 2 hours at 540 °C [117]).

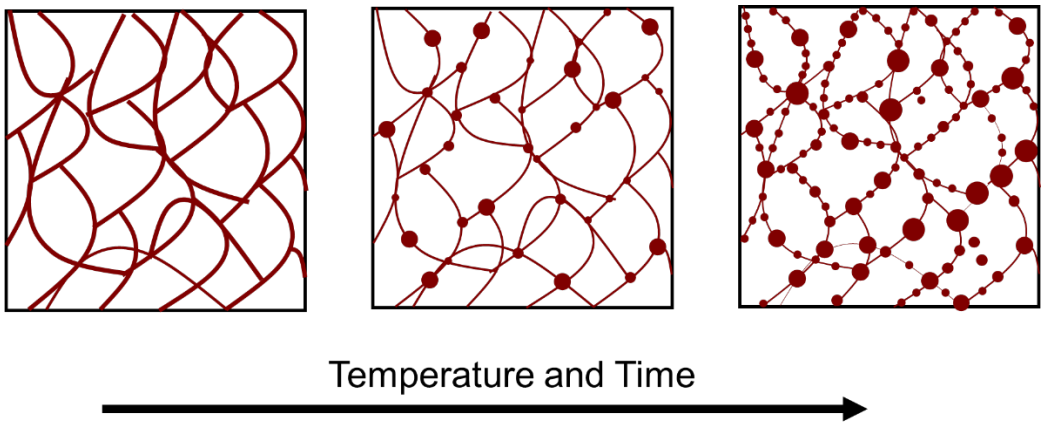

Figure 7. Schematic of the microstructural evolution of PBF-processed samples during annealing. Si-rich areas are represented as red. Adapted from Ref. [75] with permission from Elsevier.

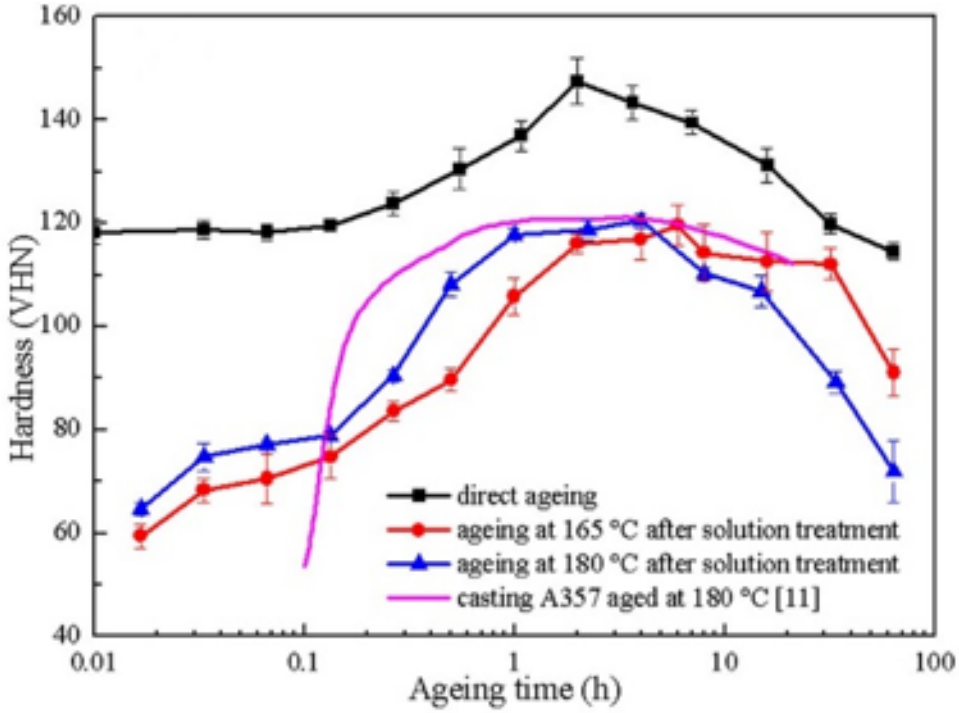

Figure 8. Hardness curves for L-PBF-processed A357 alloy, together with cast A357. Reprinted from Ref. [117] with permission from Elsevier.

In summary, both hypo and hyper-eutectic Al–Si alloys can be readily processed through L-PBF. Due to the rapid solidification of L-PBF-processed samples, the microstructure is significantly refined, which leads to increased strength in comparison with conventional casting. However, ductility and fatigue properties deteriorate, mainly due to residual stresses, porosity, unmelted particles and HAZ. The ductility of L-PBF-processed samples can be improved through appropriate heat treatment, but this is typically at the cost of strength. Therefore, it is vital to keep these advantages and disadvantages of the PBF process in mind when designing parts for real-world applications.

4 Wrought Al alloys in AM

High strength heat-treatable wrought Al-alloys (e.g. 2xxx, 6xxx and 7xxx series) are important in the aerospace and automotive industries [31, 33]. Therefore, in the last five years, these alloys have become appealing candidates for AM. However, many experimental studies have reported difficulties in processing high strength commercial wrought Al-alloys by PBF as they suffer solidification cracking/hot-cracking (**Figure 9**) [68, 123, 124]. The high volume fractions of high angle grain boundaries (HAGBs) (oriented along the build direction) and the

progressive enrichment of solute alloying elements at these boundaries over successive solidification and re-melting events (**Figure 10**), along with solid-state diffusion, causes grain boundary segregation-induced hot cracking along the boundaries [89]. Cracking phenomena in these alloys during welding have been attributed to specific characteristics, e.g. differences between solidus and liquidus temperatures, the coefficient of thermal expansion (CTE), solidification shrinkage, and poor fluidity of the molten phase [125, 126]. Further, they have relatively large freezing ranges (**Figure 11**) in comparison with the near-eutectic AlSiMg alloy (**Figure 2 (b)**). The combined effect of larger freezing ranges and solidification segregation leads to hot cracking during printing.

In the welding literature [127, 128], the cracking observed is classified in three categories: (i) during solidification (because of hot tearing), (ii) liquation type cracking (because of segregation of elements at the grain boundary), and (iii) solid-state cracking (because of stresses). This fundamental knowledge gained from conventional manufacturing processes (e.g. casting and welding) can be used to inform the development of AM. For example, it has been established that there is a correlation between the different alloying elements in Al-alloys and susceptibility to weld cracking (**Figure 12**). Interested readers can find more on the similarities between welding and AM in Ref. [2, 129].

Additionally, high strength Al alloys typically contain volatile elements (e.g. Zn, Mg, Li), which can result in an altered microstructure due to evaporation during L-PBF. It has been observed that, in certain instances [130], changes in the composition because of evaporation of certain alloying elements might even increase cracking susceptibility. In the following section, an overview of results, and some of the promising new research on high strength Al-alloys with respect to their microstructure are provided.

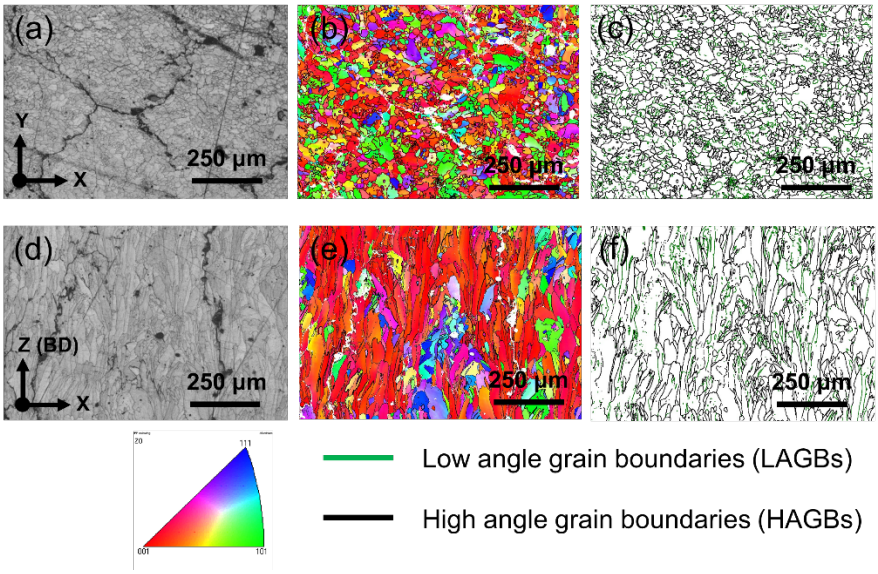

Figure 9. 2024 high strength Al alloy manufactured through L-PBF, EBSD image showing the GB distribution map of HAGBs and LAGBs showing hot cracking on some high angle grain boundaries (HAGB) [124].

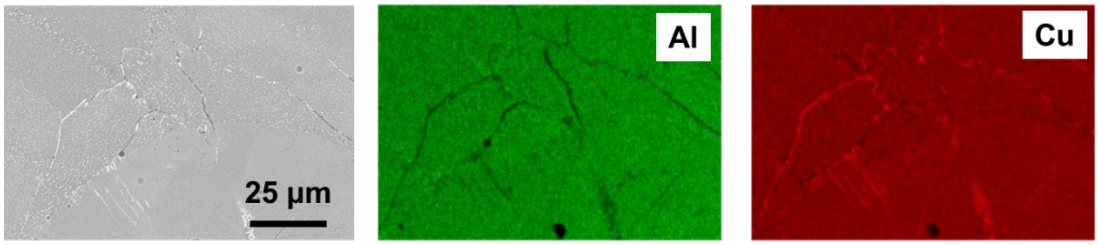

Figure 10. 2024 (Al-Cu) as printed microstructure shows strong segregation of Cu at the grain boundaries and crack initiation in these regions [124].

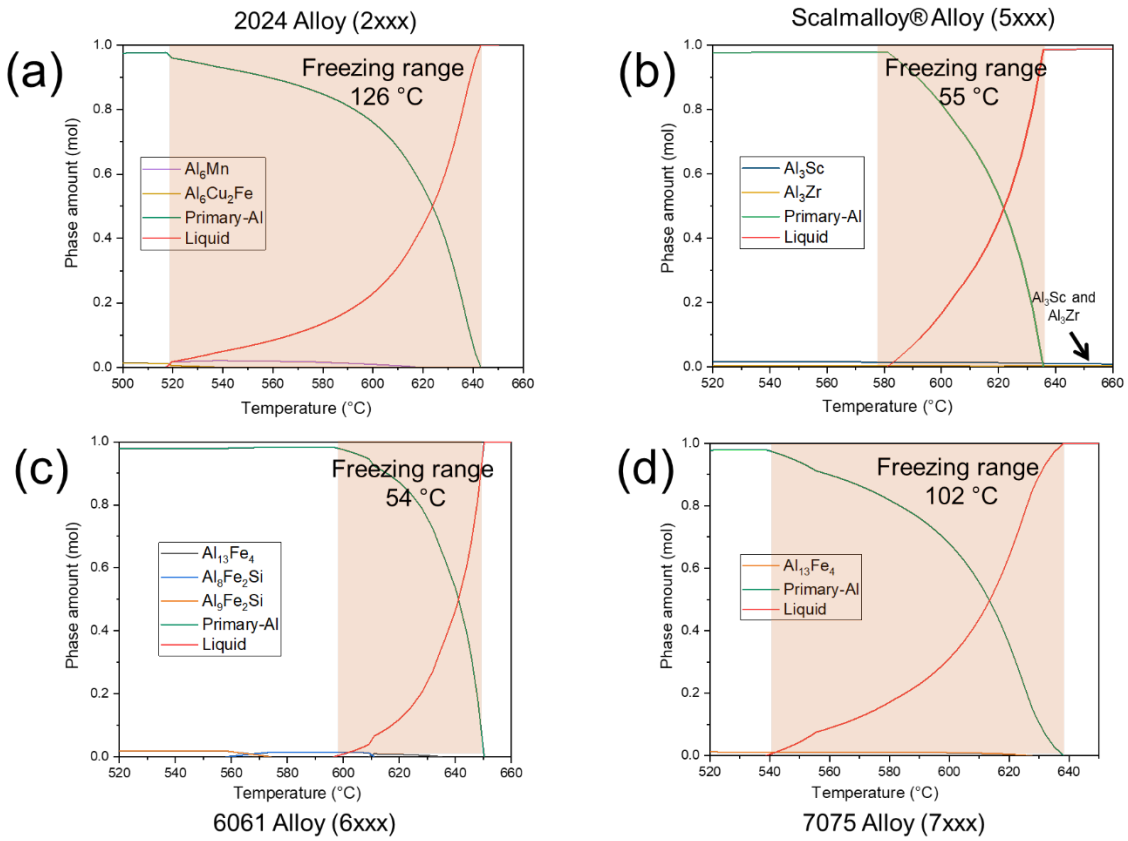

Figure 11. Thermo calc generated phase fraction evolution for (a) 2024: Al-4.35Cu-1.50Mg-0.25Fe-0.60Mn-0.08Ti-0.05Cr (2xxx) alloy, (b) Scalmalloy®: Al-4.5Mg-0.6Sc-0.5Mn-0.3 Zr (5xxx), (c) 6061: Al-0.9Mg-0.7Si-0.3Cu-0.3Fe-0.1Ti (6xxx) alloy, and (d) 7075: Al-5.5Zn-2.5Mg-1.6Cu-0.4Si-0.3Fe-0.2Cu-0.2Ti (7xxx) alloy. High strength 2xxx and 7xxx alloys have long-freezing range (> 100 °C) leading to increased hot cracking susceptibility. Phase evolution in 5xxx with Sc and Zr shows formation of Al_3Sc and Al_3Zr phases well before the primary-Al, which act as potent nucleation sites for the primary-Al, subsequently eliminating cracking during solidification. 6xxx alloys are highly crack sensitive because they contain approximately 1 wt.% Mg_2Si, which yields a higher hot cracking susceptibility according to the crack sensitivity curve (Figure 12).

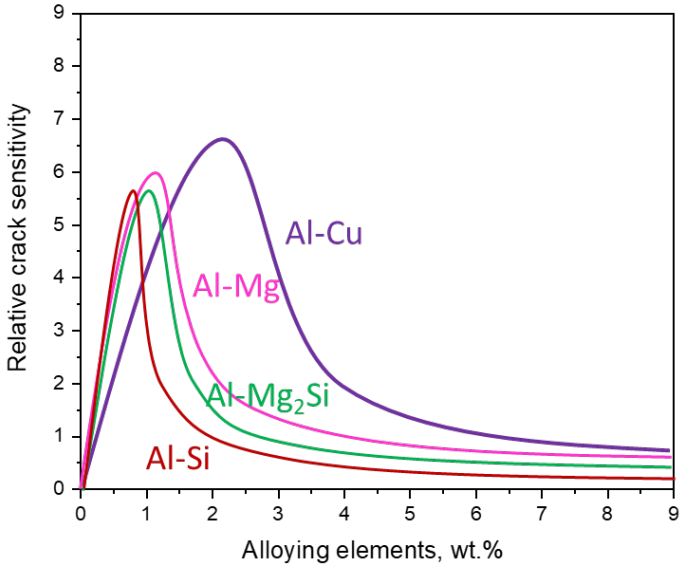

Figure 12. Effect of chemical composition of weld metal on relative crack susceptibility in various aluminium alloys [131].

4.1 **2xxx (Al-Cu)**

Al-Cu 2xxx series alloys can be precipitation hardened with high specific strength, good fracture toughness and excellent fatigue properties. Commercial 2xxx alloys contain mainly Cu and Mg elements, with the addition of Si and other minor elements such as Zn, Mn, Fe, Ti, V. Depending on the composition, an alloy may form up to the five equilibrium precipitate phases, such as θ (Al_2Cu), S ($Al_2Mg(Cu,Si,Zn)$), Si, Mg_2Si and Q ($Al_4CuMg_6Si_6$). The precipitation sequence of 2xxx alloys in the α + S phase field is [132]: SSSS (super saturated solid solution) → solute clusters → GPB (Guinier-Preston-Bagaryatsky) zones + solute clusters → GPB zones + solute clusters + S → S.

There have been various attempts to process 2xxx series alloys, such as 2022 (Al-5Cu-0.5Mg), 2024 (Al-4Cu-1Mg), 2219 (Al-6Cu-0.5Mg) and 2618 (Al-2.5Cu-1.5Mg-1Fe-1Ni), by L-PBF [26, 68, 79, 133-137]. During L-PBF, these alloys form columnar primary-Al grains with <100> texture and an extremely fine supersaturated cellular-dendritic structure. Most studies have noted that 2xxx alloys are difficult to process using L-PBF because of their high hot cracking sensitivity during the build process. Karg et al. [138] compared 2022 and 2024 alloys for L-PBF processability and concluded that the 2024 alloy yields a higher density with less susceptibility to pore formation and cracking compared to the 2022 alloy. The authors

attributed this to the higher concentration of Si in 2024, which may lead to a decrease in the melt viscosity.

A study on 2024 alloy processed under varied energy densities through modulation of scanning speed and power has been reported by Kumar et al. [124]. They observed that the occurrence of defects (including hot tearing, gas porosities, lack of fusion pores, balling, etc.) could be reduced but not completely eliminated through optimisation of processing conditions (**Figure 13**). The superheat of the melt pool was observed to be a critical factor in determining the nature of the defects. By providing increased energy input, void formation is reduced. This is because of increased melt fluidity leading to filling of shrinkage voids during solidification, which likely arises as an increased laser power at a given scan speed intensifies the thermal gradient and increases the superheated melt pool volume. However, high input energies increasing the occurrence of hot tearing. Further, the growth of columnar grains, and the liquid film between them (Cu segregation), yields susceptibility to hot cracking along the grain boundaries (**Figure 10**). Irregular fusion pores or lack of fusion defects can result from insufficient energy input, causing incomplete melting of powder and incomplete filling of the voids and gaps (Rayleigh instability) [139]. This is due to insufficient superheat in the melt pool at low laser power, reducing melt fluidity and causing incomplete filling of shrinkage voids [140].

Energy density also influences the surface roughness of the build, with a subsequent influence on the mechanical properties. In the work of Karg et al. [135] on 2219 Al alloys, samples were fabricated under preheated conditions, at temperatures of 200 ºC, where a support structure was used between the sample and base plate, in order to alleviate cracking. Here, the possibility of cracking was supressed by controlling and lowering the cooling rate during L-PBF processing, which essentially minimises heat transfer between the base plate and the sample. It was also noted that tensile properties and porosity percentage of the build are highly sensitive to the component geometry. This was attributed to the large cross-sectional area of samples on the base plate, as well as the creation of up to 5 vol.% porosity, resulting in poor tensile properties. Koutney et al. [141] studied the 2618 alloy and established a relationship between the relative density and the mechanical properties. It was observed that solidification cracks form when alloys have large freezing range due to stresses. To prevent crack formation, the thermal gradient was reduced through the use of a support structure. Using a heated platform at 400 ºC, with a lower laser scan speed, did not enhance the sample quality, but instead resulted in gas porosity. Another method used to prevent hot cracking was to increase the Si content in the

2xxx alloy, as Si promotes fluidity in the melt. Wang et al. [142] investigated Al-3.5Cu-1.5Mg-1Si alloy by adding extra Si powder produced through gas atomisation. Their work allowed fabrication of builds without any hot cracking. Tensile tests carried out on samples after build showed a yield strength of 225 MPa and an ultimate tensile strength of 370 MPa (with 5.53% elongation). The yield strength and ultimate tensile strength increased to ca. 370 MPa and ca. 460 MPa, respectively, after T6 heat treatment, but the elongation (at 6.3%) did not change significantly. They concluded that the plasticity of the samples is influenced by the formation of a *Q* phase, and that the Mg_2Si and Al_xMn_y phases are implicated in this. The formation of these phases resulted in a dimpled fracture surface. The generation of nano-Al_2Cu(Mg) precipitates in the Al matrix after T6 heat treatment was shown to offer an increased yield strength and ultimate tensile strength, compared with the as-printed samples. However, Brice et al. [143] observed Mg vaporisation during deposition, which had a significant influence on the precipitation mechanism, and they concluded that the change in Mg content led to a significant reduction in Al_2Cu (Ω) phase precipitation, resulting in poorer mechanical properties. However, it is equally important to note that adding more Si to high-strength Al-alloy degrades mechanical properties, and that the constitution of the alloy may not be suitable for structural applications. Therefore, the aim is not only to manufacture crack free components, but also to obtain good strength and ductility. This can be achieved through careful choice of alloying elements and/or potent nucleant particles.

Recently, Tan et al. [79] studied a 2024 alloy with the addition of 0.7 wt.% Ti nanoparticles to supress hot cracking and refine primary-Al grains. They demonstrated the formation of in situ Al_3Ti nanoparticles with an $L1_2$ ordered structure. After T6 heat treatment, these samples showed a tensile strength of 435 MPa with 10% elongation, which is comparable to conventionally manufactured wrought samples. Aeromet have developed the A20X™ alloys (Al-4.5Cu-0.3Mg-0.7Ag-3.5Ti) containing approximately 4.5 wt.% TiB_2 particles, which show good mechanical properties. Furthermore, Wang et al. [144] have studied Al-Cu alloy with varying amounts of Cu, noting that Al-33Cu alloy, after L-PBF processing, is seen to develop a nano-eutectic microstructure with a high compressive strength (> 1000 MPa).

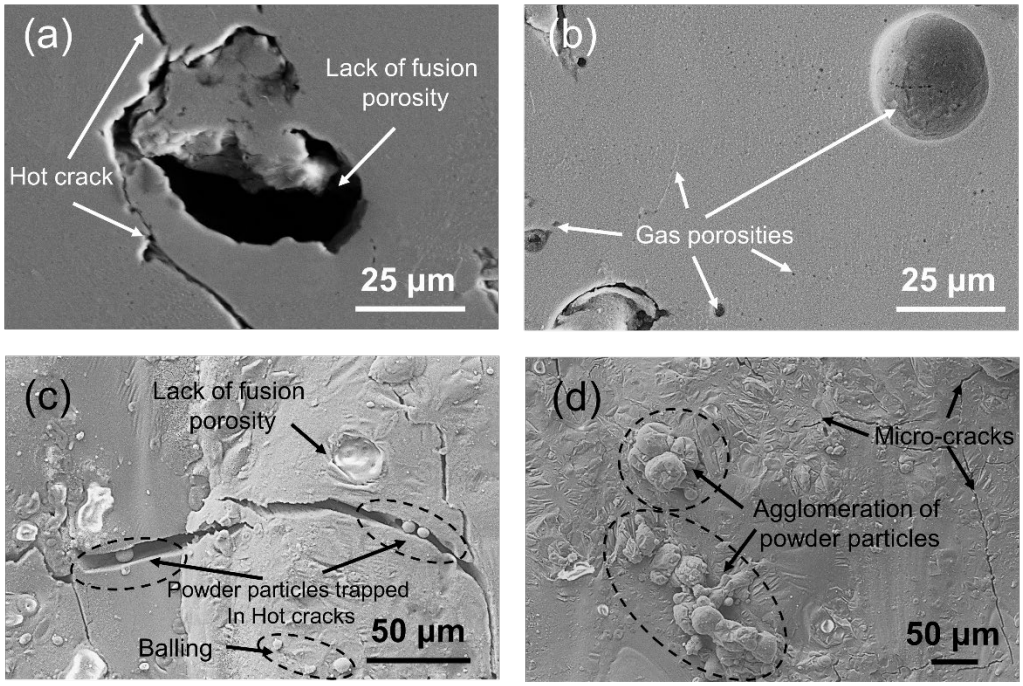

Figure 13. SEM micrographs showing various defects formed in the L-PBF processed 2024 alloy samples [124].

4.2 **5xxx (Al-Mg)**

Al-Mg-based 5xxx series alloys are not heat-treatable, however they do exhibit solid solution strengthening, strain hardening, with excellent corrosion resistance and weldability [33, 145]. Therefore, they are widely used in automotive applications, such as door assemblies. Conventionally manufactured 5xxx alloys have only moderate strength in comparison with the high-strength 2xxx, 6xxx, and 7xxx series alloys. L-PBF of Al-Mg alloy is mostly investigated with the addition of Sc and/or Zr, as small additions of these elements have shown to markedly improve relative density (up to 99.2–99.9%), yield a good combination of tensile strength and ductility, and improve overall processability [56, 69, 120, 146-149]. These elements play a dual role. Firstly, the Al_3Sc and Al_3Zr ($L1_2$ crystal structure) particles forming during solidification act as heterogeneous nucleation sites to refine the primary-Al grains, which subsequently enhances mechanical properties (Hall-Petch strengthening). This also prevents columnar grain growth that is responsible for hot cracking, which is a problem for a majority of the existing high strength Al-alloys. Secondly, the Al_3Sc and Al_3Zr nano-precipitates formed during the stress-relieving treatment (275–325 °C) promotes thermal stability of the fine grain structure during subsequent heating (150–200 °C). This is because of the slow coarsening kinetics of Al_3Sc and Al_3Zr, originating from the poor diffusivity of Sc and Zr in Al. Further, heat treatment of Sc-based alloys is basically well-matched with the broad stress-relieving treatment

of L-PBF fabricated Al alloys. Such heat treatment is a vital step before the removal of build parts from the platform, as it avoids cracking and/or deformation. This provides an additional benefit and is attractive for commercial manufacturing. Due to the advantages described here, there appears to be great promise in the development of high strength and heat-treatable Sc-Al alloys.

Schmidtke et al. [56] demonstrated the advantage of Sc alloying in combination with Zr, with a composition of Al-4.5Mg-0.66Sc-0.51Mn-0.37 Zr, for L-PBF processed AM. This alloy, also known as Scalmalloy®, was the first Al-alloy to be specifically developed for AM by the Airbus Group. Currently, Scalmalloy® is the strongest Al alloy used to consistently produce AM components of high quality, with a yield strength of 470 MPa, a tensile strength of 520 MPa, and 13% breaking elongation. Research has indicated that the precipitation of Al_3Sc leads to increased strength, with increments of ca. 40–50 MPa per 0.1 wt.% of Sc content. Li et al. [125][150] studied the alloy Al-*x*Mg-Sc-Zr by varying Mg content from 1.5 to 6 wt.%, with a reduced amount of Sc compared to Scalmalloy®. The objective of the study was to reduce the amount of expensive Sc, whilst achieving a similar performance. However, a microstructural study revealed that hot cracking was apparent when Mg content was increased. Hot cracking was only reduced when 1.3 wt.% Si was added, which yielded refined Al-Mg_2Si interdendritic eutectic structures. The microstructures consisted of ultra-fine solidification cells with diameters of 300–600 nm, with Al_3(Sc,Zr) nanoparticles 2–15 nm embedded inside the cells. The intergranular Al-Mg_2Si eutectic, with Mg_2Si diameters of ca. 10–100 nm, was present in the cell or columnar sub-grain boundary. The tensile strength of the as-printed alloy was between 500–550 MPa, with an approximate elongation of 8–11%, which was dependent on heat treatment aging process. Croteau et al. [146] studied two ternary alloys (Al-3.60Mg-1.18Zr and Al-3.66Mg-1.57Zr), intending to reduce cost by eliminating Sc while achieving equivalent grain refinement. The as-printed microstructure showed two types of grain: interconnected bands of fine (ca. 0.8 μm), equiaxed, isotropic grains, and coarser (ca. 1–10 μm), columnar, textured grains. Both grain structures contained oxide particles and Al_3Zr precipitates, providing a mixture of high yield strength (354 MPa), ultimate tensile strength (380 MPa) and ductility (ca. 20%), with isotropic properties in both as-built and peak-aged samples.

4.3 **6xxx (Al-Mg-Si)**

Heat treatable wrought 6xxx (Al–Mg–Si) Al-alloys exhibit moderate high strength (>300 MPa) with excellent corrosion resistance and extrudability, making them attractive for structural and automotive applications [31, 53, 151]. The basic precipitation sequence for the 6xxx series (in Cu free) alloys is [114, 152]: SSSS (super saturated solid solution) → solute clusters → GPB zones → metastable β′′→ metastable β′→ stable β (Mg_2Si). However, the susceptibility of Al-Mg-Si alloys to hot cracking is well known in the welding literature, and more recently in the context of laser welding. Similar to welding, L-PBF processing of crack-free builds has seen only limited success in the reported literature. The 6061 (Al-1Mg-1Si) alloy is widely studied due to its frequent use in automotive applications in the form of rolled and extruded profiles. Fulcher et al. [153] studied AA6061 alloy and compared it with printable AlSi10Mg. Their systematic experimental work concluded that hot cracking occurs in AA6061 alloy mainly due to the higher coefficient of thermal expansion (CTE) and a large freezing range. Other researchers [154-157] have also observed cracking in multiple grains and identified oxide film on grain boundaries as the major contributor to this phenomena. Researchers argue that the stable Al oxide films have a higher melting point than the Al, and during the L-PBF processing these oxide film segregate in the melt pool boundary, subsequently forming cracks. In order to improve processability of this alloy, several strategies have been explored. Robert et al. [98] prepared AA6061 alloy by mixing Al and Si powder, and their work demonstrated a reduction in hot cracking. However, mixing powders generates a slightly different chemical composition in comparison with the commercial AA6061 alloy. Martin et al. [73] studied AA 6061 alloy with addition of a grain refiner, using Zr nanoparticles to reduce hot cracking in L-PBF. Their results shown that altering primary Al-grain morphology from columnar to equiaxed (~ 5 μm in size) completely eliminate hot cracking. The Zr nanoparticles react with Al and form Al_3Zr particles, which act as nucleation sites for primary-Al grains, as explained in Section 5. Another approach that researchers have explored is heating the base plate up to 500 °C, which reduces residual stress during the build and supresses hot cracking [82]. After T6 heat treatment, crack-free builds were obtained with a tensile strength of ca. 310 MPa and an elongation of 3.5%. This is comparable with parts produced by conventional processing, but with a reduced ductility.

4.4 **7xxx (Al-Zn)**

The Al-Zn-based 7xxx alloy series is known for excellent mechanical properties, and is widely used in aerospace applications. The basic precipitation sequence for 7xxx series alloys is [158]: SSSS (super saturated solid solution) → solute clusters → GPB zones → metastable η′→ stable η ($MgZn_2$). However, as with the 2xxx and 6xxx series alloys, 7xxx has hot cracking problems during the L-PBF process. Several studies have looked at the influence of processing conditions on the formation of defects in L-PBF parts using 7075 (Al-5Zn-1.5Cu-2.5Mg) (or analogous) alloy. Si addition can prevent the formation of microcracks in 7075 alloy builds fabricated by L-PBF. For example, Sistiaga et al. [159] observed that mixing 7075 powder with 4 wt.% silicon particles eliminated microcrack formation (**Figure 16 (o, p)**). The authors attributed the improved processability to a reduced viscosity of the melt pool due to the addition of Si. They also observed a new eutectic phase and strong grain refining effect preventing the formation and propagation of cracks. Aversa et al. [160] studied 7075 alloy mixed with printable AlSi10Mg alloy (50:50), and Otani et al. [161, 162] studied 7075 alloy with 5 wt.% additional Si. Their results also confirmed that addition of Si eliminates hot cracking and forms fine primary–Al grains. However, mixing two or more powders could cause an inhomogeneous element distribution, yielding anisotropic mechanical properties within the build parts. Otani and Sasaki [162] studied pre-alloyed 7075 with up to 16 wt.% Si to elucidate the effect of Si on processing, microstructure formation and mechanical properties. Their result showed that, under optimal processing conditions, defects such as voids and hot cracking were reduced, and the relative density increased, with increasing Si content. Addition of 5 wt. % Si completely eliminated hot cracking, and achieved 360 MPa YS and 537 MPa UTS with 9.7% elongation to failure. However, they observed that large additions of Si increased brittleness. This system will likely be useful for building lightweight components by L-PBF, therefore further study of Si addition in this system could yield breakthroughs in the field.

Another approach that has been proposed is the addition of Zr or Sc. These behave as intermetallic forming elements in Al alloys. For example, Martin et al. [73] demonstrated that the use of hydrogen-stabilised Zr nanoparticles in 7075 alloy powder leads to the formation of well-dispersed Al_3Zr intermetallics. Then, during solidification, these would act as nucleation sites for primary Al, yielding finely equiaxed grains that suppress microcrack formation. The observed mechanical properties after T6 heat treatment were 325–373 MPa YS, 383–417 MPa UTS with 3.8–5.4% elongation to failure, which is close to conventionally produced 7075 alloy. Qi et al. [163] have studied 7050 alloy by altering three types of melt pool: goblet,

semicircle, and a combination of the two. The shapes are similar to the shape of keyhole, conduction, and transition modes. Their experimental results demonstrated that under the keyhole mode, the number of cracks are reduced because of the changing thermal gradient and growth rate from the melt pool boundary to the centre of the melt pool. It is also worth remembering that increasing the heat input by altering processing conditions has several disadvantages, such as evaporation of alloying elements like Zn, which can lead to chemical heterogeneities within the build. This changing melt pool strategy is equally applicable to other alloy systems. Mauduit et al. [130] studied the change in chemical composition of 7075 alloy before and after build, and noted that Zn wt.% reduced from 5.8 to 3.9 wt.% and Mg from 2.6 to 2.1 wt .%. Loss of Zn and Mg could lead to a deterioration in the mechanical properties of the 7075 alloy as these alloying elements stimulate solid solution strengthening and precipitation hardening from the $MgZn_2$ phase. Further, Kaufmann et al. [164] studied 7075 alloy by preheating the base plate at 200 °C, however their results did not show a significant reduction in hot cracking.

5 Grain refinement in additive manufacturing

A significant challenge in AM is to prevent columnar primary-Al grain structure formation during solidification. The AM process sees high thermal gradients and high cooling rates, which typically yield directional growth, and partial re-melting of previously deposited material, leading to epitaxial growth of columnar grains. Intergranular hot tearing can occur due to weaknesses arising from long solute-rich liquid channels between these grains due to thermal stress and solidification shrinkage [123]. Columnar grains also yield anisotropy in mechanical properties, which is typically undesirable [2]. A more desirable outcome is a homogeneous, fine, equiaxed grain structure which yields structures with isotropic mechanical properties that can resist hot tearing [165]. However, it is difficult to alter the build grain structure of AM components in contrast with conventionally-manufactured high-strength Al-alloys, where solidified grain structure can be rectified by subsequent thermo-mechanical processing improving the overall properties of these alloys [166]. Accordingly, in AM the best approach is to induce the formation of desired equiaxed grains during solidification, which can be achieving through modulation of the thermal gradient and solidification speed (**Figure 14)** [62, 63, 68].

In the literature, development of fine equiaxed grain structure has been demonstrated through: (i) addition of a grain refiner (e.g. TiB_2 [167], NiB [34]) and solute (e.g. Ti) [168], (ii)

application of physical force (e.g. ultrasonication [42], electromagnetic stirring [47]), and (iii) alteration of solidification conditions (e.g. cooling rate) [50, 51].

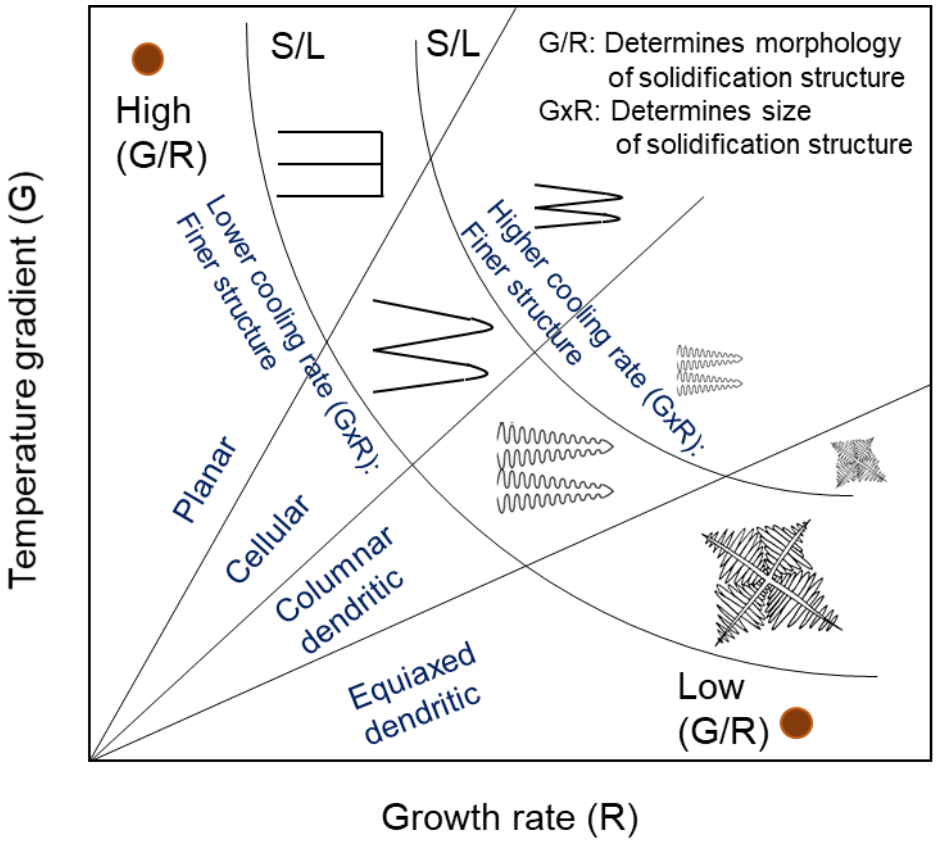

Figure 14. The effect of temperature gradient and growth rate (i.e. interface velocity) on grain size and morphology. S and L stand for solid and liquid, respectively [62, 63].

5.1 **Grain refinement by inoculant particles and solute elements**

The most common grain refining approach in conventional casting is to add trace amounts of solute and inoculants without affecting the original alloy chemistry. In 1952, Turnbull and Vonnegut [169] proposed the grain refining potency of nucleant agents through lattice disregistry. Subsequently, several experimental and mathematical models were developed to determine suitable nucleant particles for the grain refining of Al-Alloys. For example, the 'free growth model' [170] has been frequently employed to analyse the potency of nucleant particles. Similarly, in 1954, Winegard and Chalmers [171] suggested a new columnar to equiaxed transition (CET) theory, which describes the addition of inoculant agents or addition of solutes and manipulation of solidification parameters. In that direction, significant research activity has focused specifically on Al and Mg alloys. Some solute elements have an effective growth restricting factor ($Q = mC_0(k-1)$), where m is the slope of the liquidus line, C_0 is the solute

concentration in the bulk alloy, and k is the partition coefficient) [168]. Based on experimental results, it was observed that size and morphology of the grain is directly related to the solute present in the alloys. The StJohn group's extensive work concluded that, for constitutional supercooling to commence, it is vital for potential nucleant particles to instigate waves of heterogeneous nucleation well before the solid growth front during solidification [68, 172]. When there is a larger Q, supercooled zones develop before the solidification front [173]. Nucleation commences in these supercooled zones, since nucleant particles with low critical undercooling are present. The particles in these zones have coherent crystallographic matching with the matrix grains. **Figure 15** illustrates the Q value versus the grain size of Al alloys that have been conventionally cast [174]. When there is a difference in solidification conditions between conventional casting and metal AM, there will be a strong effect on the solutes and inoculant agents in promoting heterogeneous nucleation. This information can be used in metal AM in order to promote CET, where parameters such as G and R are controlled. The development of the various grain morphologies during solidification are shown in **Figure 14**. Recently in AM research [68, 73, 79, 175], the addition of solutes and inoculants has been implemented in metal AM in order to achieve equiaxed microstructures, minimising the effect of hot tearing. The objective is to introduce nucleants as either externally added particles, or by the formation of intermetallics from previously melted layers, which act as nucleation sites during subsequent solidification, or by adding high Q-value elements to generate constitutional supercooling for nucleation ahead of the solid-liquid interface.

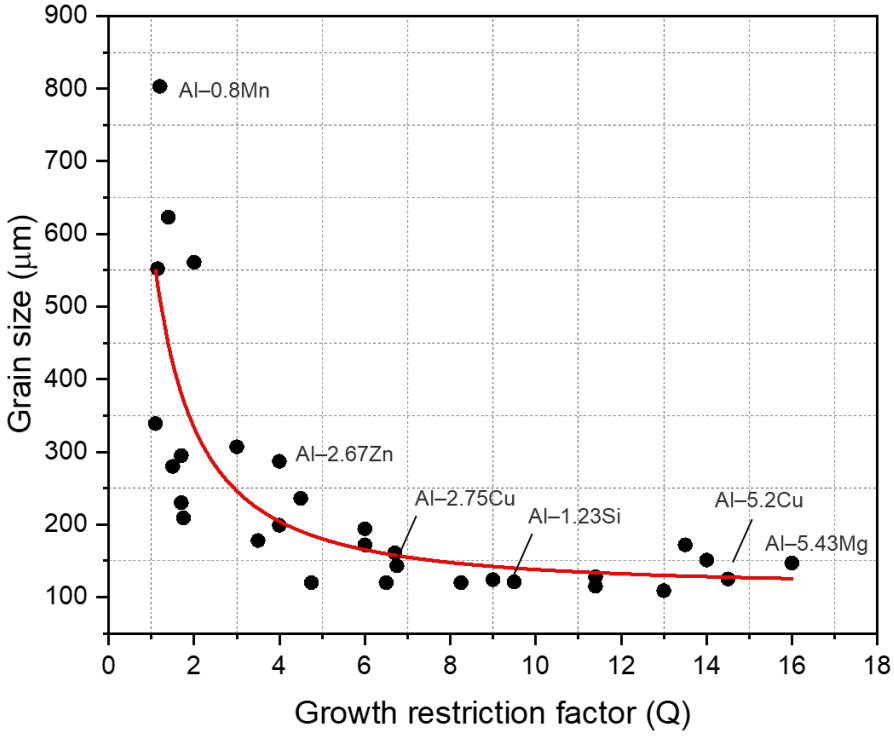

Figure 15. Primary Al grain size versus growth restriction Factor (Q), with varying alloying elements. Adapted from Ref. [174] with permission from Elsevier.

5.1.1 ***Addition of TiB_2 and solute Ti***

In the last three years, many researchers have added commonly used primary-Al grain refiners, for example Al-Ti-B master alloy, which usually have a Ti content above the TiB_2 stoichiometric ratio of 2.2:1 (wt.%) [167, 174, 176]. Therefore, this grain refiner provides TiB_2 inoculant particles as well as Ti solute, which has a comparatively high *Q* value in Al alloys. TiB_2 inoculant particles, when reacting with liquid Al, form a more stable Al_3Ti layer on TiB_2, which can act as a nucleation site for primary-Al grains. The inoculant Al-Ti-B refiners achieve grain refinement in castings (transforming mm size grains to hundreds of microns in size), therefore they are also added to AM metals to achieve the same effect. Effective grain refinement of AlSi10Mg processed by L-PBF was achieved by dispersion of nanoscale TiB_2 (5.6 wt.%) in the coating powder, as shown in **Figure 16 (a, b)** [175]. Carluccio et al. [177] studied the addition of 0.33 wt.% Al-5Ti-1B grain refiner into Al7Si-6061 alloys, where the alloys were then exposed to laser re-melting, and observed grain refinement for all the scans studied. With a low scan speed, there was a reduction in average grain size from 33 µm to 5

μm for 6061 alloy, and from 30 μm to 10 μm for Al7Si alloy. Further, Wang et al. [178] used in situ fabrication methods for L-PBF of TiB_2/Al3.5Cu1.5MgSi composite incorporating TiB_2 powder particles with a 5 vol.%, and noted significant grain refinement from 23 μm to 2.5 μm. Wen et al. [179] added 3 wt.% TiB_2 into the 2024 alloy and achieved equiaxed structures. The grain sizes were refined to 20–35 μm, and the mechanical properties of the components were enhanced, in contrast to columnar structures with length of 60 μm to 1.6 mm without the addition of TiB_2. Tan et al. [79] used Ti nanoparticles in 2024 alloy feedstock powder, which allowed the development of metastable $L1_2$-Al_3Ti. These metastable nanoparticles form because of fast cooling during L-PBF. This process was effective in initiating heterogeneous nucleation of the primary-Al, which resulted in the development of fine equiaxed structures, where the average grain size was measured to ca. 2 μm (**Figure 16 (e, f)**. Tan et al. [180, 181] also studied by adding LaB_6 addition up to 2 wt.% in the AlSi10Mg alloy (**Figure 16 (c, d)**. Their results showed that LaB_6 nanoparticles act as nucleation sites for primary-Al and refine the microstructure. The addition over 0.5 wt.% further reduced grain size, but also reduced ductility due to segregation of an excessive amount of LaB_6 particles on the grain boundaries.

5.1.2 *Addition of Zr*

Effective grain refinement has been achieved through the addition of Zr due to the formation of Al_3Zr particles through a peritectic reaction, which provides heterogeneous nucleation sites for the primary-Al grains [182]. Compared with Ti, the *Q* value of Zr is lower, however, Al_3Zr particles are still considered effective grain refiners. Zr retained in the Al solid solution also forms Al_3Zr precipitates during heat treatment, which is beneficial to the mechanical properties of Al-alloys, especially at high temperatures. Zhang et al. [133] studied 2024 (Al-Cu-Mg) alloy with the addition of 2 wt.% Zr, and they achieved elimination of hot cracking by altering the grain morphology **Figure 16 (g, h)**. As printed microstructure exhibited formation of equiaxed grains (1–2 μm in size) in the melt pool boundary, and columnar grains growing toward the centre of the melt pool. The tensile properties of this modified microstructure achieved ca. 450 MPa UTS, with low elongation to failure (2.7%). This reduction of ductility could be attributes to excessive Al_3Zr intermetallic particle formation. A study by Nie et al. [183] demonstrated that decreasing Zr content from 2 wt.% to 0.6 wt.% improved ductility of 2024 alloy up to 11%. However, addition of only 0.6 wt.% Zr is not sufficient to refine the entire microstructure, and is not capable of eliminating hot cracking in L-PBF. Additionally, it was noted that the amount of equiaxed grains that form in builds depends on the scan speed, where fully equiaxed structures were observed with a scan speed of 5 m/min, but with a scan speed of 15 m/min a

mixed columnar and equiaxed microstructure was observed [133]. Research carried out by Martin et al. [73], where they coated 7075 and 6061 alloy powders with ZrH_2 nanoparticles, showed a transformation from columnar to equiaxed grains **Figure 16 (m, n)**, where the ZrH_2 nanoparticles chemically reacted with Al and formed Al_3Zr particles . These nanoparticles were seen to not only change grain morphology but also to eliminate hot cracking, which was observed without nanoparticles in the build. This crack free build showed UTS of ca. 400 MPa in T6 condition, with a ductility below 6%. Research on 5xxx with addition of Zr (Al-Mg-Zr, also called Addalloy™) showed grain refinement on the melt pool boundary, while coarse columnar grains were seen in the melt pool [133, 148, 183]. In-depth characterisation revealed that primary Al_3Zr precipitates (100–400 nm) were responsible for the fine and equiaxed grains, while the columnar grain did not show Al_3Zr nucleants particles, which is mainly due to Zr solute trapping from increased solidification velocities. However, this non-uniformity can be reduced by applying multiple scans [147]. This change was attributed to a shallower melt pool from re-melting of the columnar grain and forming equiaxed grains from the original scan.

5.1.3 *Addition of Sc*

Additions of Sc have also been shown to achieve significant grain refinement, especially for Al-Mg alloys. As with Zr addition, the Sc yields fine equiaxed grains at the melt pool boundary, with columnar grains growing toward the centre of the pool. However, processing conditions can also affect the evolution of the microstructure as well as equiaxed grain structures [120]. Sc in AM alloys tends to have a high solid solubility within the Al-matrix, with increased cooling rates further allowing precipitation of nanoscale coherent Al_3Sc particles with appropriate heat treatment [184]. Yang et al. [148] showed that an increase in the build plate temperature up to 200 °C yielded an overall increase in volume fraction of equiaxed grains, but that the volume fraction was less when the build platform temperature was at 35 °C. It was also observed that the volumetric density of equiaxed grain structures increased when temperatures were high. **Figure 16 (i to l)** illustrates the columnar structures without the presence of Sc, and the difference when Sc is added, where uniform equiaxed grain structures are formed on the build plate when heated to 200 °C [148]. Shi et al. [120] observed a similar effect of base plate heating, however they did not observe an equiaxed microstructure. For Al-6Zn-2Mg alloy with 1 wt.% (Sc+Zr), Zhou et al. [185] observed grain refinement due to the presence of Sc and Zr, with equiaxed grains present at the melt pool boundary and columnar grains towards the centre. The presence of equiaxed grains around the re-melt boundaries appears to occur since these regions are where the temperature is kept at ca. 800 °C and

nanoscale Al_3Sc precipitates are stable. In the thermodynamic calculation of the phase development in Scalmalloy®, as shown in **Figure 10 (b)**, Al_3Sc and Al_3Zr phases are predicted to form prior to the primary-Al phase. If temperatures exceed 800 °C in the melt pool regions, the Al_3Sc precipitates exhibit metastability, resulting in columnar growth. Alloys that contain Sc tend to exhibit low Q values, therefore the development of constitutional supercooling can be insufficient to supress columnar growth, especially if the thermal gradient is relatively high. However, the phenomena of grain refinement (through Al_3Sc) at the re-melt boundaries is beneficial for supressing the effect of hot tears.

In summary, a large number of the available high strength Al-alloy powders were not designed specifically for the AM process. Most of these Al-alloys were designed for Direct Chill (DC) casting and a given set of thermo-mechanical processing routes (e.g. homogenisation–solution heat treatment, rolling, and extrusion) to achieve the desired properties. Therefore, the use of existing conventional alloys may lead to various defects under the rapid solidification. For that reason, it is essential to incorporate specific additives to existing alloys to alter their solidification behaviour or design new high strength Al-alloys by considering the thermo-chemical and thermo-mechanical aspects of the PBF process to minimise defect formation and resist columnar primary-Al growth [7]. In the literature, two approaches are explored: (i) tailor powders *ex-situ* before processing by adding alloying elements like Sc, Zr, and (ii) *in-situ* during printing by adding elements like Si, Ti (micro- and nano-size particles) for the purpose of controlling defects and grain refinement. The main selection criteria for alloying elements and alloy design are:

(i) reducing defects by improving fluidity of the melt pool e.g. Si,
(ii) grain refinement (columnar to equiaxed transition, CET) by forming or providing nucleation sites such as Al_3Sc, Al_3Zr, Al_3Ti, Al_3Nb, and ZrH for primary-Al,
(iii) phase selection during the peritectic or eutectic reaction,
(iv) alloy solidification characteristics and solid-state transformations that reduce the brittle temperature range during AM processing,
(v) providing precipitation strengthening (ideally through a stress-relieving anneal).

A preferable option is to add alloying elements within the powder feedstock (*ex-situ*), which provides chemical and microstructural uniformity. However, the nano-functionalisation approach (*in-situ*) also has number of advantages [7] e.g., pre-inoculant material can be supplied and homogeneously participate in the solidification process, nanoparticles that do not melt during printing can be introduced as nucleant particles or to produce metal matrix

composite (MMC), and feasibility studies can be carried out without specialised batches of powders.

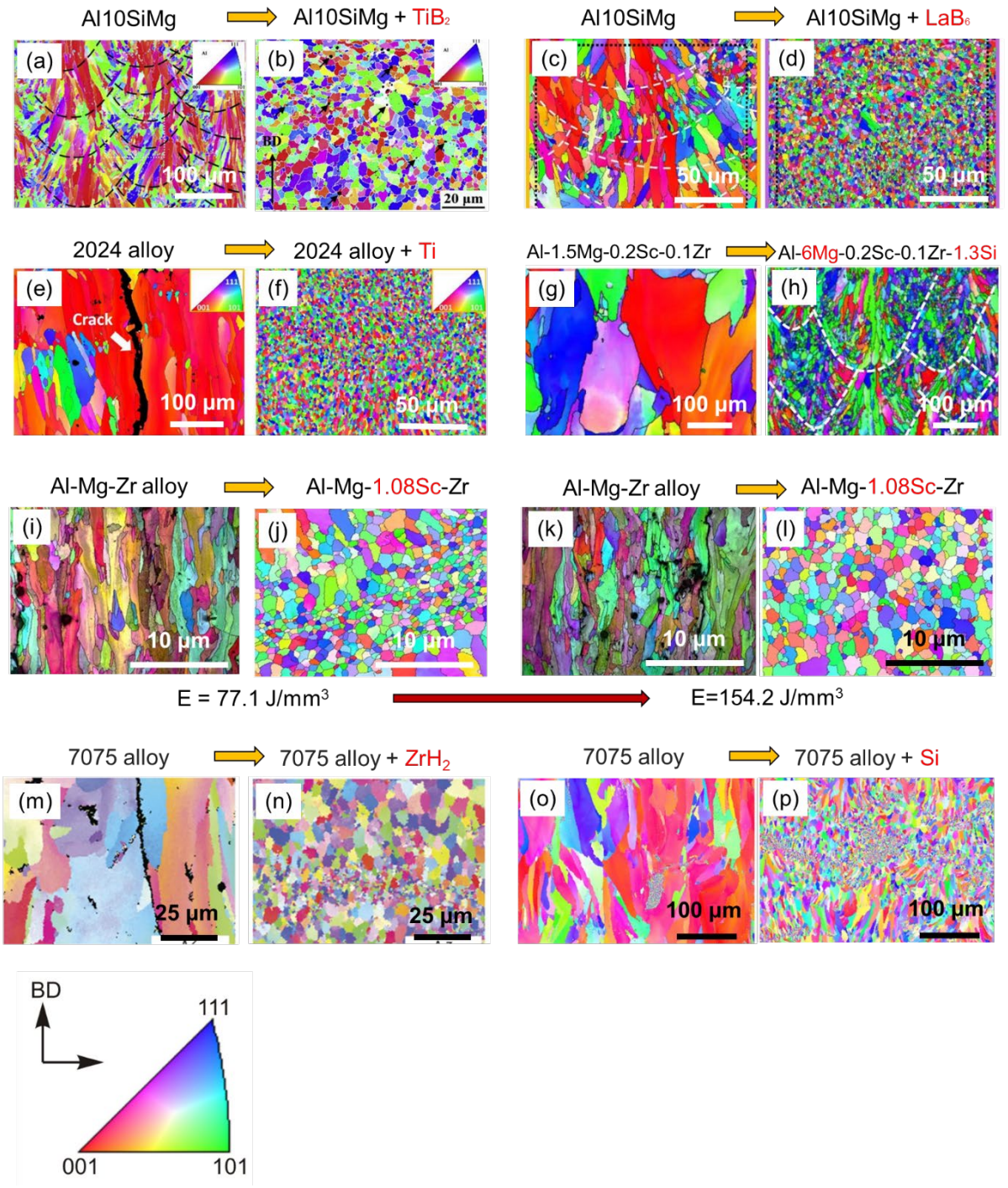

Figure 16. Grain refinement of Al alloys by solute and nucleant particle addition in L-PBF. (a,b) AlSi10Mg with and without TiB_2 [175]. (c,d) AlSi10Mg with and without LaB_6 [180, 181]. (e, f) 2024 alloy with and without Ti [79]. (g,h) Al-1.5Mg- 0.2Sc-0.1Zr with and without addition of Si and higher Mg [150]. (i to l) Al-Mg-Zr with and without Sc with different energy densities [148]. (m,n) 7075 alloy with and without ZrH_2 [73] (o,p) 7075 with and without addition of Si [159].

5.2 **Grain refining by physically induced force**

Significant research has been conducted on applying external forces such as ultrasonic [39-43], shearing [44-46] and electromagnetic [47-49] in conventional casting to achieve a refined and uniform microstructure without addition of a chemical grain refiner. In casting, widespread adaptation of the external field is restricted by the difficulty in treating large volumes of melt without contaminating the alloy. However, the melt pool is relatively small (ca. 0.1–1.0 mm in width) in AM, and overall exposure time is less [68]. In welding research, many techniques such as high intensity ultrasonication [186], energy source oscillation and energy source pulsing have been used to refine microstructure and eliminate hot cracking [186, 187]. In contrast, there have only been a handful of studies carried out in AM using Al, Ti, Ni, steel and Mg alloys. Zhang et al. [188] studied AlSi12 using ultrasound, and noted an increase in relative density from 95.4% to 99.1%, a reduction in grain size from 277.5 μm to 87.5 μm, and considerable improvement in tensile properties. Todaro et al. [189] studied a vibrating build plate (20 kHz, 30 μm amplitude), and clearly demonstrated that columnar grains are replaced with fine equiaxed grains. Although both of these studies showed promising results, builds cannot be clamped down with such approaches, which is a necessity to avoid distortion. Moreover, the application of a physical field such as ultrasound or vibration could be problematic in L-PBF based fabrication. An alternative route therefore must be explored, for example, studying the feasibility of inserting an ultrasonic sonotrode directly into the melt pool (similar to wire arc welding), which will allow the AM build plate to be clamped. Another possible route is oscillation of the heat source, which can produce frequencies of ca. 20 Hz, and 1–2 mm amplitudes in welding. Experimental results have demonstrated that this technique can reduce grain size, increase uniformity of weld pool, and suppress hot cracking in various Al alloys [187].

5.3 **Grain refinement by alteration of scanning strategy**

Several studies [88, 89, 91, 92, 141, 147, 190] have explored scanning strategies during the L-PBF fabrication process. The incentive of these studies was ultimately to reduce porosity and residual stresses through enhancing build density. However, few experimental works have shown that the scanning strategy can influence microstructure in Al-alloys [88]. In L-PBF processing, the crystal texture and microstructural evolution can be modulated by manipulating the hatch spacing and layer thickness, as these parameters directly affect partial re-melting of neighbouring tracks [147]. These digital controls during solidification are capable of yielding

microstructures with fine equiaxed grains, without hot cracking [89]. For example, Thijs et al. [88] demonstrated this concept with AlSi10Mg alloys by altering the thermal gradient during solidification. They noted that the angle or direction of scanning has a strong influence in L-PBF, an example being that when the scanning direction angle is set at 90° between the layers, the texture is significantly reduced and a weak cubic texture along the build direction arises [88]. However, further work is needed with more alloys, combined with simulation, also keeping in mind any adverse effects of drastically altering scanning strategy. In addition, it is essential to carry out detailed study to understand microstructure evolution in PBF by linking geometry and scanning strategies considering spatial variations of G and R. It is worth mentioning that scanning strategy alone may not be capable of controlling solidification texture because of the misalignment between the solidification growth direction and the dominant heat flow direction, and other complexities of metallic systems [2].

6 Al powder feedstocks for AM

Powder feedstock properties play a key role in the eventual quality of an AM-processed part, unlike other powder metallurgical processes [191]. Powder size, shape and distribution are the most important characteristics that determine suitability in L-PBF [192]. These can directly influence powder flow, packing density, melt pool character, surface roughness, defects, bulk density and mechanical properties [191-193]. Therefore, it is essential to have consistent powder characteristics that ensure consistent and reliable performance of the final build. Tan et al. [191] have carried out an in-depth literature review on powder feedstocks for AM, covering individual powder characteristic and their influence on the build.

The main routes to the manufacture of Al metal powders are gas atomisation and plasma atomisation in inert gas environments, such as Ar, He and N [194]. Probably the most widely used method is gas atomisation for Al, as it is less expensive compared to the plasma. However, reports on plasma atomisation describe a higher sphericity and uniformity in size, which is ultimately favourable for PBF [191]. The obtained spherical powders had much better flowability and laser absorption relative to the raw powder. The characteristics of Al-alloy powders can be modulated by varying the atomisation conditions and by modifying the atomisation techniques.

Currently, the most widely available powder feedstock for Al alloys are based on commercially available Al alloys, except the alloys like Scalmalloy® , which is an AM specific alloy and

available on the market from designated suppliers. Unfortunately, powder feedstocks are typically expensive and do not come in many varieties, with only a few common alloys being available as powder, a situation which hinders the uptake of Al-alloys for application in AM. A viable alternative is to blend these commercially available powder feedstocks to yield final products of a desired alloy composition. However, the inhomogeneity in the composition and resultant microstructural features are not desirable.

6.1 **Effect of powder morphology on AM**

In powder metallurgy, it is thought that the powder size distribution has the strongest influence on packing behaviour, versus other powder characteristics. Different powder sizes are used for the different L-PBF process. For example, recommended powder sized for the laser based process is 15-45 μm diameter and for e-beam process is 45 to 106 μm diameter, [195]. Powder grades with a wide particle size distribution (PSD) and acceptable amounts of fine particles will typically yield high packing densities [192]. PSD can change at various stages after atomisation, for example, during storage, during L-PBF processing (spreading), and during powder recycling, which obviously influences feedstock behaviour [196]. There have been many mathematical models proposed to study powder packing in relation to PSD, with the aim of increasing packing density [197, 198].

Studies have shown that when there is higher packing efficiency, there is a general reduction of the number of void interstices in coarse powder matrices (**Figure 17)**. Adding fine particles fills the pores found in loose granular networks, which improves packing efficiency. There can be an increase in packing density from 74–84% (**Figure 17 (a)**) following the addition of fine particles equivalent to the size of its inter-particle voids [192, 199]. Addition of a third component can further decrease any voids, thus a high packing density of 95.7% is achievable. Olakanmi et al. [200] worked with various multimodal blends in Al powders, where it was noted in a tri-modal blend comprising of coarse/medium/fine particle sizes, with a ratio of 5:2:1 and 75:20:5 wt.%, revealed an increase in tapped density by 3 wt.% compared to biomodal grades with fine particles sizes of 10–14 μm. The sphericity and morphology of the particles are of importance, since this can affect the powder packing density. Muñiz-Lerma et al. [201] studied AlSi7Mg powder with three different size distributions, and concluded that fine particles facilitate water absorption and powder cohesion due to high surface energies, which is ultimately linked to spreading and defects. However, when a narrow PSD and particles larger than 48 μm were used, a reduced water absorption and powder cohesion improved powder flow

and density. PSD is also known to have a significant effect on the laser–powder interaction. Larger particles require higher laser energies to induce melting, while smaller particles, with their greater surface area, assist with the densification kinetics. Generally, there appears to be a direct correlation between the powder bed density and the part density, with powders possessing a wider range of particle sizes providing a higher powder bed density and generating higher-density parts under low laser energy intensities [191]. Aboulkhair et al. [100] studied AlSi10Mg powders with two different morphologies (elongated versus spherical), and demonstrated that the spherical powder can achieve a higher relative density (99.6%) compared to the elongated powder (97.74%), under identical conditions. However, the elongated powder is also capable of producing high-density builds, but requires careful optimisation. This is one of the key challenges to build high quality components with consistency. Furthermore, PSD and powder sphericity change when the powder is recycled. This is because irregular aggregates can form when some powder particles become fused but do not adhere to the build part [196, 202]. This is particularly problematic for repeated build cycles, where PSD and sphericity changes are likely to disturb flow and packing performance [203]. An effective but time-consuming measure is to sieve the powder between cycles. An alternate, flowability of Al-powders (micron-sized) can achieve by surface modifications such as attaching nano-particles (silica, titania and carbon black) or chemically (methyltrichlorosilane) [204].

Currently, specific to Al-alloys, there have been very limited studies performed to establish the inter-relationship between (i) powder characteristics (size, shape, distribution, packing density, rheology), (ii) processing parameters (laser output, scanning velocity, scan strategy, and platform heating), (iii) build quality (relative density, type of defects, microstructure), and (iv) resulting mechanical properties. Further, studies focusing on the changes in packing between single- and multi-layered powder, as well as understanding the overall behaviour of the powder bed, are going to be important. Uncovering the relationships between these variables, and how they affect the final quality of the build, will be an important step towards improving methods of powder processing.

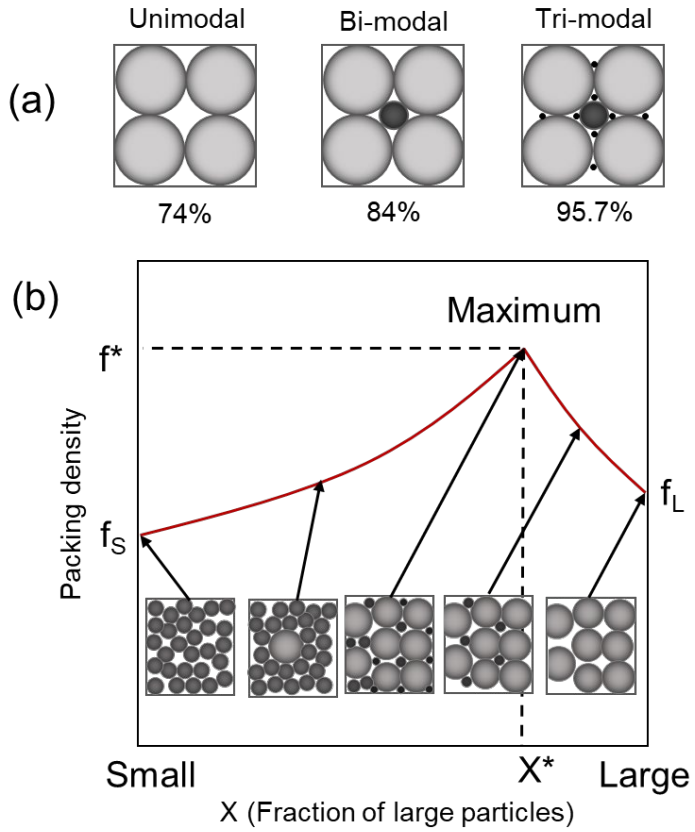

Figure 17. (a) Packing density and particle arrangement [192], and (b) particle compositions versus packing density [205] .

6.2 **Effect of contamination on AM**

Besides powder morphology, powder contamination has been an underlying issue in L-PBF. The inherent physical properties of Al alloy powder pose some challenges. These include the formation of a stable and adherent surface oxide layers and the high reflectivity and thermal conductivity of the powders. Oxide formation on Al surfaces is inevitable, governed by thermodynamics and the passivating nature of Al oxide, even though Al powder manufacture and the L-PBF process can be carried out under controlled inert conditions ($O_2 \ll 0.15\%$) [202]. Al powder particles can readily pick up contamination through adsorbed gases, moisture, organics and other inclusions that are still unavoidable [202, 206]. Oxidation hinders part consolidation through the formation of oxide skins on powder surfaces, which can induce defects, e.g. porosity and cracks, decrease the powder flowability resulting in poor powder packing density, reduce wettability generating poor adherence across formed layers, break-up of the melt pool into droplets causing balling effects and increasing the surface roughness of the part, impairing the overall mechanical properties [207]. Hu et al. [208] studied AlCu5MnCdVa alloy with different oxygen levels, and their study highlights the importance

of controlling atmospheric oxygen and its effect on mechanical properties. For Al alloys, the increment in oxygen content form large volume of oxide make component brittle. This problem can be severe, especially for thin sections or hot-cracking susceptible alloys, where formation of oxides is more significant. An additional mode of contamination comes from the formation of hydroxides because of moisture adsorption at powder surfaces, which typically occurs in humid conditions [206]. As compared to oxide layers that are solidified on the powder surface which are typically hard and brittle, adsorbate hydroxide films disrupt the flow of particles within the powder bed due to agglomeration of particles [209]. A decrease in water vapour pressure at elevated temperatures can initiate the formation of hydroxide layers, ultimately producing oxides during crystallisation. The development of oxides can modify the atmospheric condition of the chamber, for example the dissociation of hydrogen atoms during laser contact with absorbed water layers can produce gas that becomes entrapped during melt solidification, thus contributing to melt pool spattering [196]. A drying step can be used to aid in removal of residual moisture in powders, which was also reported to reduce porosity and facilitate a > 99% relative density in AlSi10Mg alloy built parts, which is greater than that obtained without the drying step, by reducing effect of oxide and hydroxide formation [103]. Currently, limited literature is available that attempts to explore and understand the severity of contamination under different powder conditions, and there needs to be further investigation to establish good standard practice to produce consistent AM builds, which is one of the bottlenecks for the uptake of Al for AM. Some standards have been published for use in the AM industry, but there is still a lack of known standards specific to Al-alloys.

7 Conclusions

Al is the second most important metal after steel due to its excellent strength-to-weight ratio and corrosion resistance. Because of these advantages, along with its manufacturability and affordability, Al is one of the most attractive materials for aerospace and automotive applications, in comparison with other materials like titanium and composites. Recent works published on AM with Al reflect the opportunity and challenges of this manufacturing pathway. In the current literature, near eutectic AlSiMg alloys have been studied in depth, starting from material feedstock through to real-life component performance. However, the amount of research on high-strength Al-alloys remains low, because of the hot cracking challenge associated with alloy solidification under the high cooling rates, as experienced in AM

processing. Based on the literature surveyed in this review, the following conclusions can be drawn.

1) AlSiMg alloys can be easily processed through AM and can achieve almost full relative density under optimised processing conditions. However, conventional wrought Al-alloys (2xxx, 6xxx, and 7xxx) are difficult to process using L-PBF due to high hot crack sensitivity during solidification.
2) AlSiMg alloys produced through L-PBF show improved strength in comparison with their conventionally produced cast counterparts, which is mainly due to microstructural refinement under the high cooling rates and heat treatment. With high cooling rates, as-printed samples exhibit a higher solute concentration than the equilibrium values, which requires lower solution heat treatment times than typically used in conventional practice.
3) All Al-alloys form columnar primary-Al grains with <001> texture in the build direction. This directional growth in L-PBF leads to anisotropic properties. Applying a different scanning strategy, such as varying hatch style and contour, significantly changes texture and can decreases anisotropy.
4) Most wrought Al-alloy studies find that addition of Si improves alloy printability and suppresses hot cracking as a result of an improvement in melt pool fluidity.
5) Small additions of Sc and/or Zr can markedly improve the relative density, yielding a good combination of tensile strength and ductility, and overall processability. These elements achieve this in two ways: (i) by forming nucleant particles (Al_3Sc and Al_3Zr) during the solidification, refining primary-Al grains and suppressing hot cracking, and (ii) forming nano-precipitates during the aging process to improve tensile properties of alloy. AM-specific Scalmalloy® has clearly demonstrated the advantages of these elements in wrought alloys. Other grain-refining particles such as TiB_2, Al_3Ti and solutes have also shown promising results, with respects to suppressing hot cracking and improving tensile properties of the Al-alloys.
6) The low absorptivity and high thermal conductivity of Al necessitates high energy input to melt the Al powder. This leads to vaporisation of high vapor pressure elements (e.g. Zn and Mg). Loss of these elements could increase chemical heterogeneity within the L-PBF processed sample and influence solution hardening and precipitation hardening.
7) Powder characteristics (such as morphology, packing density, surface chemistry, oxygen content and hydroxides) significantly influence flowability, induce various defects and ultimately lead to low relative density and poor mechanical properties.

8 Outlook

In the future, additional research is required to overcome the challenges found in the AM with Al alloys. The challenges are both scientific and technological; some critical ones are highlighted in the Ishikawa diagram shown in **Figure 18**. Much fundamental work needs to be carried out to link solidification science and process metallurgy. Accordingly, there are a number of areas which future research should focus on.

Currently, most high-strength Al-alloy research is focused on readily available commercial alloys, which were designed for completely different processing routes. In PBF, these alloys experience rapid and repeated thermal cycling, which leads to the occurrence of common defects such as hot cracking, lack of fusion, loss of alloying elements through vaporisation, residual stresses and undesirable microstructural character. In order to take advantage of rapid solidification in PBF, there is a critical need to design AM-specific high strength, high performance, and cost-effective Al-alloys, which exploit the unique features of AM to generate superior properties in comparison with their conventional counterparts. An example is the high cooling rate in conjunction with the repeated heating, which allows a high level of precipitation and dispersoid particle formation. This can be useful for the grain refining, as well yielding improved mechanical properties. New alloys must be designed by understanding geometry-alloying-processing-property-performance relationships, in order to meet industrial demands in terms of the consistency in manufacturing and performance.

Furthermore, it is clear from all previous studies that in order to achieve fine and equiaxed grains in high strength Al alloys in AM, it is essential to have potent nucleant or grain refiner inoculant particles, either externally added, or which form during the build with high Q value solute elements. It is necessary to find commercially viable routes to incorporate and uniformly distribute these particles and/or elements in an appropriate amount within the powder feedstock. Future research can explore the effects of scanning strategy, physically-induced force and chemical inoculation, which may provide desirable microstructures and mechanical properties for commercial requirements.

Many existing Al AM challenges can be handled using numerical simulation, digital twins and machine learning, and with closed-loop monitoring and control systems. The combination of well-thought-out experiments and simulations can significantly reduce trial and error in testing, which will ultimately allow us to create a reliable printing database for the benefit of all.

In-depth research needs to be performed on the role of Al powder feedstock, starting with increasing the production throughput of high-quality powders with suitable morphology to achieve optimal powder behaviour during the PBF process. In the literature, there is only limited understanding of how powder characteristics influence process conditions and subsequent mechanical properties of PBF-processed samples. Also, it is equally important to create a strategy for how different grades of powders can be recycled, handled and re-used without affecting processing and performance of the build.

Al AM research will be significantly beneficial if the research is carried out in close collaboration with both ends of the supply chain (powder manufacturers and end users), and it will rapidly put fundamental developments into practice and should enhance knowledge in the area of Al AM.

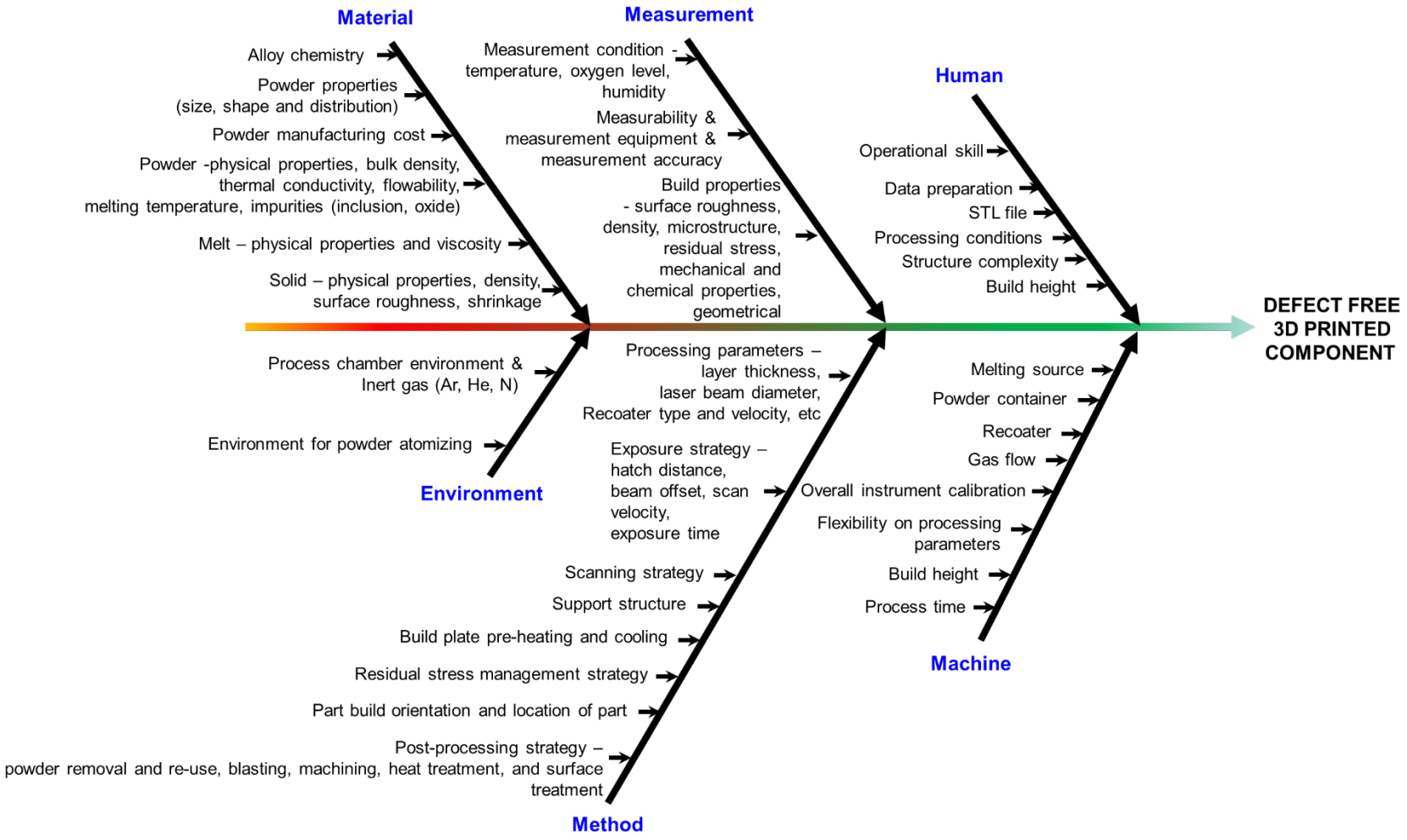

Figure 18. An Ishikawa diagram, illustrating the key scientific and technological challenges in metal additive manufacturing.

Acknowledgment

Dr Hiren Kotadia would like to thank the WMG HVM Catapult centre for funding this work.

References

[1] S. Lathabai, Chapter 2 - Additive Manufacturing of Aluminium-Based Alloys and Composites, in: R.N. Lumley (Ed.), Fundamentals of Aluminium Metallurgy, Woodhead Publishing2018, pp. 47-92.
[2] T. DebRoy, H.L. Wei, J.S. Zuback, T. Mukherjee, J.W. Elmer, J.O. Milewski, A.M. Beese, A. Wilson-Heid, A. De, W. Zhang, Additive manufacturing of metallic components – Process, structure and properties, Progress in Materials Science 92 (2018) 112-224.
[3] D.D. Gu, W. Meiners, K. Wissenbach, R. Poprawe, Laser additive manufacturing of metallic components: materials, processes and mechanisms, International Materials Reviews 57(3) (2012) 133-164.
[4] D. Herzog, V. Seyda, E. Wycisk, C. Emmelmann, Additive manufacturing of metals, Acta Materialia 117 (2016) 371-392.
[5] S.A.M. Tofail, E.P. Koumoulos, A. Bandyopadhyay, S. Bose, L. O'Donoghue, C. Charitidis, Additive manufacturing: scientific and technological challenges, market uptake and opportunities, Materials Today 21(1) (2018) 22-37.
[6] M. Attaran, The rise of 3-D printing: The advantages of additive manufacturing over traditional manufacturing, Business Horizons 60(5) (2017) 677-688.
[7] T.M. Pollock, A.J. Clarke, S.S. Babu, Design and Tailoring of Alloys for Additive Manufacturing, Metallurgical and Materials Transactions A 51(12) (2020) 6000-6019.
[8] W.J. Sames, F.A. List, S. Pannala, R.R. Dehoff, S.S. Babu, The metallurgy and processing science of metal additive manufacturing, International Materials Reviews 61(5) (2016) 315-360.
[9] X. Tan, Y. Kok, Y.J. Tan, M. Descoins, D. Mangelinck, S.B. Tor, K.F. Leong, C.K. Chua, Graded microstructure and mechanical properties of additive manufactured Ti–6Al–4V via electron beam melting, Acta Materialia 97 (2015) 1-16.
[10] L.E. Murr, E.V. Esquivel, S.A. Quinones, S.M. Gaytan, M.I. Lopez, E.Y. Martinez, F. Medina, D.H. Hernandez, E. Martinez, J.L. Martinez, S.W. Stafford, D.K. Brown, T. Hoppe, W. Meyers, U. Lindhe, R.B. Wicker, Microstructures and mechanical properties of electron beam-rapid manufactured Ti–6Al–4V biomedical prototypes compared to wrought Ti–6Al–4V, Materials Characterization 60(2) (2009) 96-105.
[11] E. Wycisk, S. Siddique, D. Herzog, F. Walther, C. Emmelmann, Fatigue Performance of Laser Additive Manufactured Ti–6Al–4V in Very High Cycle Fatigue Regime up to 109 Cycles, Frontiers in Materials 2(72) (2015).
[12] A.M. Beese, B.E. Carroll, Review of Mechanical Properties of Ti-6Al-4V Made by Laser-Based Additive Manufacturing Using Powder Feedstock, JOM 68(3) (2016) 724-734.
[13] D. Cormier, O. Harrysson, T. Mahale, H. West, Freeform Fabrication of Titanium Aluminide via Electron Beam Melting Using Prealloyed and Blended Powders, Research Letters in Materials Science 2007 (2007) 034737.
[14] D. Srivastava, I.T.H. Chang, M.H. Loretto, The effect of process parameters and heat treatment on the microstructure of direct laser fabricated TiAl alloy samples, Intermetallics 9(12) (2001) 1003-1013.
[15] K.N. Amato, S.M. Gaytan, L.E. Murr, E. Martinez, P.W. Shindo, J. Hernandez, S. Collins, F. Medina, Microstructures and mechanical behavior of Inconel 718 fabricated by selective laser melting, Acta Materialia 60(5) (2012) 2229-2239.
[16] J.F. Wang, Q.J. Sun, H. Wang, J.P. Liu, J.C. Feng, Effect of location on microstructure and mechanical properties of additive layer manufactured Inconel 625 using gas tungsten arc welding, Materials Science and Engineering: A 676 (2016) 395-405.

[17] H.E. Helmer, C. Körner, R.F. Singer, Additive manufacturing of nickel-based superalloy Inconel 718 by selective electron beam melting: Processing window and microstructure, Journal of Materials Research 29(17) (2014) 1987-1996.
[18] G.P. Dinda, A.K. Dasgupta, J. Mazumder, Laser aided direct metal deposition of Inconel 625 superalloy: Microstructural evolution and thermal stability, Materials Science and Engineering: A 509(1) (2009) 98-104.
[19] K. Mumtaz, N. Hopkinson, Selective laser melting of Inconel 625 using pulse shaping, Rapid Prototyping Journal 16(4) (2010) 248-257.
[20] M. Rombouts, G. Maes, M. Mertens, W. Hendrix, Laser metal deposition of Inconel 625: Microstructure and mechanical properties, Journal of Laser Applications 24(5) (2012) 052007.
[21] A.G. Demir, B. Previtali, Additive manufacturing of cardiovascular CoCr stents by selective laser melting, Materials & Design 119 (2017) 338-350.
[22] N.V. Kazantseva, I.V. Ezhov, D.I. Davydov, A.G. Merkushev, Analysis of Structure and Mechanical Properties of Co–Cr–Mo Alloy Obtained by 3D Printing, Physics of Metals and Metallography 120(12) (2019) 1172-1179.
[23] P. Bajaj, A. Hariharan, A. Kini, P. Kürnsteiner, D. Raabe, E.A. Jägle, Steels in additive manufacturing: A review of their microstructure and properties, Materials Science and Engineering: A 772 (2020) 138633.
[24] A. Yadollahi, N. Shamsaei, S.M. Thompson, D.W. Seely, Effects of process time interval and heat treatment on the mechanical and microstructural properties of direct laser deposited 316L stainless steel, Materials Science and Engineering: A 644 (2015) 171-183.
[25] I.M. Kusoglu, B. Gökce, S. Barcikowski, Research trends in laser powder bed fusion of Al alloys within the last decade, Additive Manufacturing 36 (2020) 101489.
[26] N.T. Aboulkhair, M. Simonelli, L. Parry, I. Ashcroft, C. Tuck, R. Hague, 3D printing of Aluminium alloys: Additive Manufacturing of Aluminium alloys using selective laser melting, Progress in Materials Science 106 (2019) 100578.
[27] C. Panwisawas, Y.T. Tang, R.C. Reed, Metal 3D printing as a disruptive technology for superalloys, Nature Communications 11(1) (2020) 2327.
[28] S.M.H. Hojjatzadeh, N.D. Parab, W. Yan, Q. Guo, L. Xiong, C. Zhao, M. Qu, L.I. Escano, X. Xiao, K. Fezzaa, W. Everhart, T. Sun, L. Chen, Pore elimination mechanisms during 3D printing of metals, Nature Communications 10(1) (2019) 3088.
[29] Word Aluminium Organisation (2020).
[30] Aluminium in cars: unlocking the light-weighting potential, European Aluminium Association (2020).
[31] J. Davis, ASM Specialty Handbook: Aluminum and Aluminum Alloys, ASM International (1993).
[32] D. Raabe, C.C. Tasan, E.A. Olivetti, Strategies for improving the sustainability of structural metals, Nature 575(7781) (2019) 64-74.
[33] I. Polmear, Light Alloys: From Traditional Alloys to Nanocrystals, 4th Edition, Butterworth-Heinemann (2005).
[34] M. Nowak, L. Bolzoni, N. Hari Babu, Grain refinement of Al–Si alloys by Nb–B inoculation. Part I: Concept development and effect on binary alloys, Materials & Design (1980-2015) 66 (2015) 366-375.
[35] X. Liu, Y. Wu, X. Bian, The nucleation sites of primary Si in Al–Si alloys after addition of boron and phosphorus, Journal of Alloys and Compounds 391(1) (2005) 90-94.
[36] P.B. Crosley, L.F. Mondolfo, The modification of Aluminium-Silicon alloys, Mod Cast 49(63) (1966).
[37] K. Nogita, S.D. McDonald, K. Tsujimoto, K. Yasuda, A.K. Dahle, Aluminium phosphide as a eutectic grain nucleus in hypoeutectic Al-Si alloys, Microscopy 53(4) (2004) 361-369.
[38] C.R. Ho, B. Cantor, Heterogeneous nucleation of solidification of Si in Al-Si and Al-Si-P alloys, Acta Metallurgica et Materialia 43(8) (1995) 3231-3246.
[39] G.I. Eskin, D.G. Eskin, Ultrasonic treatment of light alloys metals, 2nd Edition CRS Press (2014).

[40] A. Das, H.R. Kotadia, Effect of high-intensity ultrasonic irradiation on the modification of solidification microstructure in a Si-rich hypoeutectic Al–Si alloy, Materials Chemistry and Physics 125(3) (2011) 853-859.
[41] H.R. Kotadia, A. Das, Modification of solidification microstructure in hypo- and hyper-eutectic Al–Si alloys under high-intensity ultrasonic irradiation, Journal of Alloys and Compounds 620(Supplement C) (2015) 1-4.
[42] H.R. Kotadia, M. Qian, D.G. Eskin, A. Das, On the microstructural refinement in commercial purity Al and Al-10wt% Cu alloy under ultrasonication during solidification, Materials & Design 132(Supplement C) (2017) 266-274.
[43] H.R. Kotadia, M. Qian, A. Das, Microstructural modification of recycled aluminium alloys by high-intensity ultrasonication: Observations from custom Al–2Si–2Mg–1.2Fe–(0.5,1.0)Mn alloys, Journal of Alloys and Compounds 823 (2020) 153833.
[44] H.R. Kotadia, N. Hari Babu, H. Zhang, Z. Fan, Microstructural refinement of Al–10.2%Si alloy by intensive shearing, Materials Letters 64(6) (2010) 671-673.
[45] H.R. Kotadia, E. Doernberg, J.B. Patel, Z. Fan, R. Schmid-Fetzer, Solidification of Al-Sn-Cu Based Immiscible Alloys under Intense Shearing, Metallurgical and Materials Transactions A 40(9) (2009) 2202-2211.
[46] H.R. Kotadia, N. Hari Babu, H. Zhang, S. Arumuganathar, Z. Fan, Solidification Behavior of Intensively Sheared Hypoeutectic Al-Si Alloy Liquid, Metallurgical and Materials Transactions A 42(4) (2011) 1117-1126.
[47] S. Nafisi, D. Emadi, M.T. Shehata, R. Ghomashchi, Effects of electromagnetic stirring and superheat on the microstructural characteristics of Al–Si–Fe alloy, Materials Science and Engineering: A 432(1) (2006) 71-83.
[48] T. Campanella, C. Charbon, M. Rappaz, Grain refinement induced by electromagnetic stirring: A dendrite fragmentation criterion, Metallurgical and Materials Transactions A 35(10) (2004) 3201-3210.
[49] C. Vives, Electromagnetic refining of aluminum alloys by the CREM process: Part I. Working principle and metallurgical results, Metallurgical Transactions B 20(5) (1989) 623-629.
[50] A.N. Lakshmanan, S.G. Shabestari, J.E. Gruzleski, Microstructure control of iron intermetallics in Al-Si casting alloys, Z. Metallkd. 86(7) (1995) 457-67.
[51] A.M. Samuel, A. Pennors, C. Villeneuve, F.H. Samuel, H.W. Doty, S. Valtierra, Effect of cooling rate and Sr-modification on porosity and Fe-intermetallics formation in Al-6.5% Si-3.5% Cu-Fe alloys, International Journal of Cast Metals Research 13(4) (2000) 231-253.
[52] J.D. Robson, O. Engler, C. Sigli, A. Deschamps, W.J. Poole, Advances in Microstructural Understanding of Wrought Aluminum Alloys, Metallurgical and Materials Transactions A 51(9) (2020) 4377-4389.
[53] W.S. Miller, L. Zhuang, J. Bottema, A.J. Wittebrood, P. De Smet, A. Haszler, A. Vieregge, Recent development in aluminium alloys for the automotive industry, Materials Science and Engineering: A 280(1) (2000) 37-49.
[54] E.A. Jägle, Z. Sheng, L. Wu, L. Lu, J. Risse, A. Weisheit, D. Raabe, Precipitation Reactions in Age-Hardenable Alloys During Laser Additive Manufacturing, JOM 68(3) (2016) 943-949.
[55] L.J. Gibson, M.F. Ashby, Cellular Solids: Structure and Properties, Cambridge Univ. Press, Cambridge (1997).
[56] K. Schmidtke, F. Palm, A. Hawkins, C. Emmelmann, Process and Mechanical Properties: Applicability of a Scandium modified Al-alloy for Laser Additive Manufacturing, Physics Procedia 12 (2011) 369-374.
[57] C. Suryanarayana, Rapid Solidification Processing, in: K.H.J. Buschow, R.W. Cahn, M.C. Flemings, B. Ilschner, E.J. Kramer, S. Mahajan, P. Veyssière (Eds.), Encyclopedia of Materials: Science and Technology, Elsevier, Oxford, 2002, pp. 1-10.
[58] W. Kurz, B. Giovanola, R. Trivedi, Theory of microstructural development during rapid solidification, Acta Metallurgica 34(5) (1986) 823-830.

[59] M. Das, V.K. Balla, D. Basu, S. Bose, A. Bandyopadhyay, Laser processing of SiC-particle-reinforced coating on titanium, Scripta Materialia 63(4) (2010) 438-441.
[60] B. Zheng, Y. Zhou, J.E. Smugeresky, J.M. Schoenung, E.J. Lavernia, Thermal Behavior and Microstructural Evolution during Laser Deposition with Laser-Engineered Net Shaping: Part I. Numerical Calculations, Metallurgical and Materials Transactions A 39(9) (2008) 2228-2236.
[61] E.J. Lavernia, J.D. Ayers, T.S. Srivatsan, Rapid solidification processing with specific application to aluminium alloys, International Materials Reviews 37(1) (1992) 1-44.
[62] J.D. Hunt, Solidification and casting of metals, The Metals Society, London (1979) 3-9.
[63] D.M. Stefanescu, R. Ruxanda, Fundamentals of Solidification Metallography and Microstructures, in: G.F. Vander Voort (Ed.), ASM International2004, pp. 1-24.
[64] A. Tonejc, X-ray study of the decomposition of metastable Al-rich Al-Fe solid solutions, Metallurgical Transactions 2(2) (1971) 437-440.
[65] M. Ruhr, E.E. Lavernia, J.C. Baram, Extended Al(Mn) solution in a rapidly solidified Al-Li-Mn-Zr alloy, Metallurgical Transactions A 21(6) (1990) 1785-1789.
[66] E.O. Hall, The Deformation and Ageing of Mild Steel: III Discussion of Results, Proceedings of the Physical Society. Section B 64(9) (1951) 747-753.
[67] N.J. Petch, The cleavage strength of polycrystals, J. Iron Steel Inst. 174 (1953) 25–28
[68] D. Zhang, A. Prasad, M.J. Bermingham, C.J. Todaro, M.J. Benoit, M.N. Patel, D. Qiu, D.H. StJohn, M. Qian, M.A. Easton, Grain Refinement of Alloys in Fusion-Based Additive Manufacturing Processes, Metallurgical and Materials Transactions A 51(9) (2020) 4341-4359.
[69] A.B. Spierings, K. Dawson, M. Voegtlin, F. Palm, P.J. Uggowitzer, Microstructure and mechanical properties of as-processed scandium-modified aluminium using selective laser melting, CIRP Annals 65(1) (2016) 213-216.
[70] W.E. King, A.T. Anderson, R.M. Ferencz, N.E. Hodge, C. Kamath, S.A. Khairallah, A.M. Rubenchik, Laser powder bed fusion additive manufacturing of metals; physics, computational, and materials challenges, Applied Physics Reviews 2(4) (2015) 041304.
[71] M. Wang, B. Song, Q. Wei, Y. Zhang, Y. Shi, Effects of annealing on the microstructure and mechanical properties of selective laser melted AlSi7Mg alloy, Materials Science and Engineering: A 739 (2019) 463-472.
[72] N. Read, W. Wang, K. Essa, M.M. Attallah, Selective laser melting of AlSi10Mg alloy: Process optimisation and mechanical properties development, Materials & Design (1980-2015) 65 (2015) 417-424.
[73] J.H. Martin, B.D. Yahata, J.M. Hundley, J.A. Mayer, T.A. Schaedler, T.M. Pollock, 3D printing of high-strength aluminium alloys, Nature 549 (2017) 365.
[74] L. Zhuo, Z. Wang, H. Zhang, E. Yin, Y. Wang, T. Xu, C. Li, Effect of post-process heat treatment on microstructure and properties of selective laser melted AlSi10Mg alloy, Materials Letters 234 (2019) 196-200.
[75] K.G. Prashanth, S. Scudino, H.J. Klauss, K.B. Surreddi, L. Löber, Z. Wang, A.K. Chaubey, U. Kühn, J. Eckert, Microstructure and mechanical properties of Al–12Si produced by selective laser melting: Effect of heat treatment, Materials Science and Engineering: A 590 (2014) 153-160.
[76] X.P. Li, X.J. Wang, M. Saunders, A. Suvorova, L.C. Zhang, Y.J. Liu, M.H. Fang, Z.H. Huang, T.B. Sercombe, A selective laser melting and solution heat treatment refined Al–12Si alloy with a controllable ultrafine eutectic microstructure and 25% tensile ductility, Acta Materialia 95 (2015) 74-82.
[77] N. Kang, P. Coddet, C. Chen, Y. Wang, H. Liao, C. Coddet, Microstructure and wear behavior of in-situ hypereutectic Al–high Si alloys produced by selective laser melting, Materials & Design 99 (2016) 120-126.
[78] P. Ma, K.G. Prashanth, S. Scudino, Y. Jia, H. Wang, C. Zou, Z. Wei, J. Eckert, Influence of Annealing on Mechanical Properties of Al-20Si Processed by Selective Laser Melting, Metals 4(1) (2014) 28-36.

[79] Q. Tan, J. Zhang, Q. Sun, Z. Fan, G. Li, Y. Yin, Y. Liu, M.-X. Zhang, Inoculation treatment of an additively manufactured 2024 aluminium alloy with titanium nanoparticles, Acta Materialia 196 (2020) 1-16.
[80] F. Belelli, R. Casati, F. Larini, M. Riccio, M. Vedani, Investigation on two Ti–B-reinforced Al alloys for Laser Powder Bed Fusion, Materials Science and Engineering: A 808 (2021) 140944.
[81] Q. Jia, P. Rometsch, S. Cao, K. Zhang, X. Wu, Towards a high strength aluminium alloy development methodology for selective laser melting, Materials & Design 174 (2019) 107775.
[82] S.Z. Uddin, L.E. Murr, C.A. Terrazas, P. Morton, D.A. Roberson, R.B. Wicker, Processing and characterization of crack-free aluminum 6061 using high-temperature heating in laser powder bed fusion additive manufacturing, Additive Manufacturing 22 (2018) 405-415.
[83] A. Aversa, G. Marchese, A. Saboori, E. Bassini, D. Manfredi, S. Biamino, D. Ugues, P. Fino, M. Lombardi, New Aluminum Alloys Specifically Designed for Laser Powder Bed Fusion: A Review, Materials (Basel) 12(7) (2019) 1007.
[84] N. Kang, P. Coddet, H. Liao, C. Coddet, Macrosegregation mechanism of primary silicon phase in selective laser melting hypereutectic Al – High Si alloy, Journal of Alloys and Compounds 662 (2016) 259-262.
[85] J. Wu, X.Q. Wang, W. Wang, M.M. Attallah, M.H. Loretto, Microstructure and strength of selectively laser melted AlSi10Mg, Acta Materialia 117 (2016) 311-320.
[86] Y. Kok, X.P. Tan, P. Wang, M.L.S. Nai, N.H. Loh, E. Liu, S.B. Tor, Anisotropy and heterogeneity of microstructure and mechanical properties in metal additive manufacturing: A critical review, Materials & Design 139 (2018) 565-586.
[87] K. Kempen, L. Thijs, J. Van Humbeeck, J.P. Kruth, Processing AlSi10Mg by selective laser melting: parameter optimisation and material characterisation, Materials Science and Technology 31(8) (2015) 917-923.
[88] L. Thijs, K. Kempen, J.-P. Kruth, J. Van Humbeeck, Fine-structured aluminium products with controllable texture by selective laser melting of pre-alloyed AlSi10Mg powder, Acta Materialia 61(5) (2013) 1809-1819.
[89] P. Kontis, E. Chauvet, Z. Peng, J. He, A.K. da Silva, D. Raabe, C. Tassin, J.-J. Blandin, S. Abed, R. Dendievel, B. Gault, G. Martin, Atomic-scale grain boundary engineering to overcome hot-cracking in additively-manufactured superalloys, Acta Materialia 177 (2019) 209-221.
[90] L.Z. Zhao, M.J. Zhao, L.J. Song, J. Mazumder, Ultra-fine Al–Si hypereutectic alloy fabricated by direct metal deposition, Materials & Design (1980-2015) 56 (2014) 542-548.
[91] H. Zhang, D. Gu, D. Dai, C. Ma, Y. Li, R. Peng, S. Li, G. Liu, B. Yang, Influence of scanning strategy and parameter on microstructural feature, residual stress and performance of Sc and Zr modified Al–Mg alloy produced by selective laser melting, Materials Science and Engineering: A 788 (2020) 139593.
[92] R.M. Gouveia, F.J.G. Silva, E. Atzeni, D. Sormaz, J.L. Alves, A.B. Pereira, Effect of Scan Strategies and Use of Support Structures on Surface Quality and Hardness of L-PBF AlSi10Mg Parts, Materials 13(10) (2020) 2248.
[93] S.R. Ch, A. Raja, P. Nadig, R. Jayaganthan, N.J. Vasa, Influence of working environment and built orientation on the tensile properties of selective laser melted AlSi10Mg alloy, Materials Science and Engineering: A 750 (2019) 141-151.
[94] P. Yang, M.A. Rodriguez, D.K. Stefan, A. Allen, D. Bradley, L. Deibler, B.H. Jared, Microstructure and Thermal Properties of Selective Laser Melted AlSi10Mg Alloy, 3rd AM Cross-JOWOG Meeting, Kansas City National Security Campus, Kansas City, MO, 2017 (2017).
[95] S.N. Grigoriev, T.V. Tarasova, G.O. Gvozdeva, S. Nowotny, Solidification behaviour during laser microcladding of Al–Si alloys, Surface and Coatings Technology 268 (2015) 303-309.
[96] E.O. Olakanmi, Selective laser sintering/melting (SLS/SLM) of pure Al, Al–Mg, and Al–Si powders: Effect of processing conditions and powder properties, Journal of Materials Processing Technology 213(8) (2013) 1387-1405.

[97] H. Rao, S. Giet, K. Yang, X. Wu, C.H.J. Davies, The influence of processing parameters on aluminium alloy A357 manufactured by Selective Laser Melting, Materials & Design 109 (2016) 334-346.
[98] C.E. Roberts, D. Bourell, T. Watt, J. Cohen, A Novel Processing Approach for Additive Manufacturing of Commercial Aluminum Alloys, Physics Procedia 83 (2016) 909-917.
[99] N.T. Aboulkhair, N.M. Everitt, I. Ashcroft, C. Tuck, Reducing porosity in AlSi10Mg parts processed by selective laser melting, Additive Manufacturing 1-4 (2014) 77-86.
[100] N.T. Aboulkhaira, I. Maskery, I. Ashcroft, C. Tuck, N.M. Everitt, The role of powder properties on the processability of Aluminium alloys in selective laser melting, Lasers in Manufacturing Conference 2015 (2015).
[101] D. Gu, Y. Shen, Balling phenomena during direct laser sintering of multi-component Cu-based metal powder, Journal of Alloys and Compounds 432(1) (2007) 163-166.
[102] C. Weingarten, D. Buchbinder, N. Pirch, W. Meiners, K. Wissenbach, R. Poprawe, Formation and reduction of hydrogen porosity during selective laser melting of AlSi10Mg, Journal of Materials Processing Technology 221 (2015) 112-120.
[103] K.V. Yang, P. Rometsch, T. Jarvis, J. Rao, S. Cao, C. Davies, X. Wu, Porosity formation mechanisms and fatigue response in Al-Si-Mg alloys made by selective laser melting, Materials Science and Engineering: A 712 (2018) 166-174.
[104] T. Kimura, T. Nakamoto, M. Mizuno, H. Araki, Effect of silicon content on densification, mechanical and thermal properties of Al-xSi binary alloys fabricated using selective laser melting, Materials Science and Engineering: A 682 (2017) 593-602.
[105] N.T. Aboulkhair, I. Maskery, C. Tuck, I. Ashcroft, N.M. Everitt, On the formation of AlSi10Mg single tracks and layers in selective laser melting: Microstructure and nano-mechanical properties, Journal of Materials Processing Technology 230 (2016) 88-98.
[106] G. Guiglionda, W.J. Poole, The role of damage on the deformation and fracture of Al–Si eutectic alloys, Materials Science and Engineering: A 336(1) (2002) 159-169.
[107] J.H. Rao, Y. Zhang, K. Zhang, X. Wu, A. Huang, Selective laser melted Al-7Si-0.6Mg alloy with in-situ precipitation via platform heating for residual strain removal, Materials & Design 182 (2019) 108005.
[108] T. Kimura, T. Nakamoto, Microstructures and mechanical properties of A356 (AlSi7Mg0.3) aluminum alloy fabricated by selective laser melting, Materials & Design 89 (2016) 1294-1301.
[109] K. Kempen, L. Thijs, J. Van Humbeeck, J.P. Kruth, Mechanical Properties of AlSi10Mg Produced by Selective Laser Melting, Physics Procedia 39 (2012) 439-446.
[110] D. Buchbinder, W. Meiners, K. Wissenbach, R. Poprawe, Selective laser melting of aluminum die-cast alloy—Correlations between process parameters, solidification conditions, and resulting mechanical properties, Journal of Laser Applications 27(S2) (2015) S29205.
[111] K.G. Prashanth, S. Scudino, J. Eckert, Defining the tensile properties of Al-12Si parts produced by selective laser melting, Acta Materialia 126 (2017) 25-35.
[112] J. Suryawanshi, K.G. Prashanth, S. Scudino, J. Eckert, O. Prakash, U. Ramamurty, Simultaneous enhancements of strength and toughness in an Al-12Si alloy synthesized using selective laser melting, Acta Materialia 115 (2016) 285-294.
[113] X.J. Wang, L.C. Zhang, M.H. Fang, T.B. Sercombe, The effect of atmosphere on the structure and properties of a selective laser melted Al–12Si alloy, Materials Science and Engineering: A 597 (2014) 370-375.
[114] G.A. Edwards, K. Stiller, G.L. Dunlop, M.J. Couper, The precipitation sequence in Al–Mg–Si alloys, Acta Materialia 46(11) (1998) 3893-3904.
[115] W.T. Donlon, Precipitation of aluminum in the silicon phase contained in W319 and 356 aluminum alloys, Metallurgical and Materials Transactions A 34(3) (2003) 523-529.
[116] K. Matsuda, D. Teguri, T. Sato, Y. Uetani, S. Ikeno, Cu Segregation around Metastable Phase in Al-Mg-Si Alloy with Cu, MATERIALS TRANSACTIONS 48(5) (2007) 967-974.
[117] J.H. Rao, Y. Zhang, K. Zhang, A. Huang, C.H.J. Davies, X. Wu, Multiple precipitation pathways in an Al-7Si-0.6Mg alloy fabricated by selective laser melting, Scripta Materialia 160 (2019) 66-69.

[118] J.H. Rao, P. Rometsch, X. Wu, C.H.J. Davies, 7 - The processing and heat treatment of selective laser melted Al-7Si-0.6Mg alloy, in: F. Froes, R. Boyer (Eds.), Additive Manufacturing for the Aerospace Industry, Elsevier2019, pp. 143-161.
[119] I. Rosenthal, R. Shneck, A. Stern, Heat treatment effect on the mechanical properties and fracture mechanism in AlSi10Mg fabricated by additive manufacturing selective laser melting process, Materials Science and Engineering: A 729 (2018) 310-322.
[120] Y. Shi, K. Yang, S.K. Kairy, F. Palm, X. Wu, P.A. Rometsch, Effect of platform temperature on the porosity, microstructure and mechanical properties of an Al–Mg–Sc–Zr alloy fabricated by selective laser melting, Materials Science and Engineering: A 732 (2018) 41-52.
[121] S. Siddique, M. Imran, E. Wycisk, C. Emmelmann, F. Walther, Influence of process-induced microstructure and imperfections on mechanical properties of AlSi12 processed by selective laser melting, Journal of Materials Processing Technology 221 (2015) 205-213.
[122] S. Siddique, M. Imran, F. Walther, Very high cycle fatigue and fatigue crack propagation behavior of selective laser melted AlSi12 alloy, International Journal of Fatigue 94 (2017) 246-254.
[123] N. Coniglio, C.E. Cross, Initiation and growth mechanisms for weld solidification cracking, International Materials Reviews 58(7) (2013) 375-397.
[124] M. Kumar, G. Gibbons, A. Das, I. Manna, D. Tanner, H.R. Kotadia, Additive manufacturing of Aluminium alloy 2024 by laser powder bed fusion: Microstructural evolution, defects and mechanical properties, Rapid Prototyping Journal, Under review (2021).
[125] I. Todd, No more tears for metal 3D printing, Nature 549(7672) (2017) 342-343.
[126] G. Mathers, 11 - Weld defects and quality control, in: G. Mathers (Ed.), The Welding of Aluminium and its Alloys, Woodhead Publishing2002, pp. 199-215.
[127] S. Kou, Library, MRS Bulletin 28(9) (2003) 674-675.
[128] S. Kou, A criterion for cracking during solidification, Acta Materialia 88 (2015) 366-374.
[129] H.L. Wei, H.K.D.H. Bhadeshia, S.A. David, T. DebRoy, Harnessing the scientific synergy of welding and additive manufacturing, Science and Technology of Welding and Joining 24(5) (2019) 361-366.
[130] A. Mauduit, S. Pillot, H. Gransac, Study of the suitability of aluminium alloys for additive manufacturing by laser powdered fuion U.P.B. Sci. Bull., Series B, 79(4) (2017).
[131] J.H. Dudas, F.R. Collins, Preventing weld cracks in high strength aluminum alloys, Welding journal 45 (1966) 241-249.
[132] G. Sha, R.K.W. Marceau, X. Gao, B.C. Muddle, S.P. Ringer, Nanostructure of aluminium alloy 2024: Segregation, clustering and precipitation processes, Acta Materialia 59(4) (2011) 1659-1670.
[133] H. Zhang, H. Zhu, X. Nie, J. Yin, Z. Hu, X. Zeng, Effect of Zirconium addition on crack, microstructure and mechanical behavior of selective laser melted Al-Cu-Mg alloy, Scripta Materialia 134 (2017) 6-10.
[134] B. Ahuja, M. Karg, K.Y. Nagulin, M. Schmidt, Fabrication and Characterization of High Strength Al-Cu Alloys Processed Using Laser Beam Melting in Metal Powder Bed, Physics Procedia 56 (2014) 135-146.
[135] M.C.H. Karg, B. Ahuja, S.V. Wiesenmayer, M. Schmidt, S.V. Kuryntsev, Effects of Process Conditions on the Mechanical Behavior of Aluminium Wrought Alloy EN AW-2219 (AlCu6Mn) Additively Manufactured by Laser Beam Melting in Powder Bed., Micromachines 8(23) (2017).
[136] O. Gharbi, D. Jiang, D.R. Feenstra, S.K. Kairy, Y. Wu, C.R. Hutchinson, N. Birbilis, On the corrosion of additively manufactured aluminium alloy AA2024 prepared by selective laser melting, Corrosion Science 143 (2018) 93-106.
[137] R. Casati, J.N. Lemke, A.Z. Alarcon, M. Vedani, Aging Behavior of High-Strength Al Alloy 2618 Produced by Selective Laser Melting, Metallurgical and Materials Transactions A 48(2) (2017) 575-579.
[138] M. Karg, B. Ahuja, S. Kuryntsev, A. Gorunov, M. Schmidt, Processability of high strength Aluminium-Copper alloys AW-2022 and 2024 by Laser Beam Melting in Powder Bed, 2014.
[139] R. Martinez, I. Todd, K. Mumtaz, In situ alloying of elemental Al-Cu12 feedstock using selective laser melting, Virtual and Physical Prototyping 14(3) (2019) 242-252.

[140] S. Coeck, M. Bisht, J. Plas, F. Verbist, Prediction of lack of fusion porosity in selective laser melting based on melt pool monitoring data, Additive Manufacturing 25 (2019) 347-356.
[141] D. Koutny, D. Palousek, L. Pantelejev, C. Hoeller, R. Pichler, L. Tesicky, J. Kaiser, Influence of Scanning Strategies on Processing of Aluminum Alloy EN AW 2618 Using Selective Laser Melting, Materials 11(2) (2018) 298.
[142] P. Wang, C. Gammer, F. Brenne, K.G. Prashanth, R.G. Mendes, M.H. Rümmeli, T. Gemming, J. Eckert, S. Scudino, Microstructure and mechanical properties of a heat-treatable Al-3.5Cu-1.5Mg-1Si alloy produced by selective laser melting, Materials Science and Engineering: A 711 (2018) 562-570.
[143] C. Brice, R. Shenoy, M. Kral, K. Buchannan, Precipitation behavior of aluminum alloy 2139 fabricated using additive manufacturing, Materials Science and Engineering: A 648 (2015) 9-14.
[144] P. Wang, L. Deng, K.G. Prashanth, S. Pauly, J. Eckert, S. Scudino, Microstructure and mechanical properties of Al-Cu alloys fabricated by selective laser melting of powder mixtures, Journal of Alloys and Compounds 735 (2018) 2263-2266.
[145] H. Zhao, D.R. White, T. DebRoy, Current issues and problems in laser welding of automotive aluminium alloys, International Materials Reviews 44(6) (1999) 238-266.
[146] J.R. Croteau, S. Griffiths, M.D. Rossell, C. Leinenbach, C. Kenel, V. Jansen, D.N. Seidman, D.C. Dunand, N.Q. Vo, Microstructure and mechanical properties of Al-Mg-Zr alloys processed by selective laser melting, Acta Materialia 153 (2018) 35-44.
[147] S. Griffiths, M.D. Rossell, J. Croteau, N.Q. Vo, D.C. Dunand, C. Leinenbach, Effect of laser rescanning on the grain microstructure of a selective laser melted Al-Mg-Zr alloy, Materials Characterization 143 (2018) 34-42.
[148] K.V. Yang, Y. Shi, F. Palm, X. Wu, P. Rometsch, Columnar to equiaxed transition in Al-Mg(-Sc)-Zr alloys produced by selective laser melting, Scripta Materialia 145 (2018) 113-117.
[149] H. Zhang, D. Gu, J. Yang, D. Dai, T. Zhao, C. Hong, A. Gasser, R. Poprawe, Selective laser melting of rare earth element Sc modified aluminum alloy: Thermodynamics of precipitation behavior and its influence on mechanical properties, Additive Manufacturing 23 (2018) 1-12.
[150] R. Li, M. Wang, Z. Li, P. Cao, T. Yuan, H. Zhu, Developing a high-strength Al-Mg-Si-Sc-Zr alloy for selective laser melting: Crack-inhibiting and multiple strengthening mechanisms, Acta Materialia 193 (2020) 83-98.
[151] M.H. Khan, A. Das, Z. Li, H.R. Kotadia, Effects of Fe, Mn, chemical grain refinement and cooling rate on the evolution of Fe intermetallics in a model 6082 Al-alloy, Intermetallics 132 (2021) 107132.
[152] A.K. Gupta, D.J. Lloyd, Study of precipitation kinetics in a super purity Al-0.8 Pct Mg-0.9 Pct Si alloy using differential scanning calorimetry, Metallurgical and Materials Transactions A 30(13) (1999) 879-890.
[153] B.A. Fulcher, D.K. Leigh, T.J. Watt, Comparison of AlSi10Mg and Al 6061 Processed Through DMLS, Proc. 25th Solid Free. Fabr. Symp (2014) 404-419.
[154] L.-E. Loh, C.-K. Chua, W.-Y. Yeong, J. Song, M. Mapar, S.-L. Sing, Z.-H. Liu, D.-Q. Zhang, Numerical investigation and an effective modelling on the Selective Laser Melting (SLM) process with aluminium alloy 6061, International Journal of Heat and Mass Transfer 80 (2015) 288-300.
[155] L.E. Loh, Z.H. Liu, D.Q. Zhang, M. Mapar, S.L. Sing, C.K. Chua, W.Y. Yeong, Selective Laser Melting of aluminium alloy using a uniform beam profile, Virtual and Physical Prototyping 9(1) (2014) 11-16.
[156] E. Louvis, P. Fox, C.J. Sutcliffe, Selective laser melting of aluminium components, Journal of Materials Processing Technology 211(2) (2011) 275-284.
[157] Y. Ding, J.A. Muñiz-Lerma, M. Trask, S. Chou, A. Walker, M. Brochu, Microstructure and mechanical property considerations in additive manufacturing of aluminum alloys, MRS Bulletin 41(10) (2016) 745-751.
[158] L.K. Berg, J. Gjønnes, V. Hansen, X.Z. Li, M. Knutson-Wedel, G. Waterloo, D. Schryvers, L.R. Wallenberg, GP-zones in Al–Zn–Mg alloys and their role in artificial aging, Acta Materialia 49(17) (2001) 3443-3451.

[159] M.L. Montero-Sistiaga, R. Mertens, B. Vrancken, X. Wang, B. Van Hooreweder, J.-P. Kruth, J. Van Humbeeck, Changing the alloy composition of Al7075 for better processability by selective laser melting, Journal of Materials Processing Technology 238 (2016) 437-445.
[160] A. Aversa, G. Marchese, D. Manfredi, M. Lorusso, F. Calignano, S. Biamino, M. Lombardi, P. Fino, M. Pavese, Laser Powder Bed Fusion of a High Strength Al-Si-Zn-Mg-Cu Alloy, Metals 8(5) (2018) 300.
[161] Y. Otani, Y. Kusaki, K. Itagaki, S. Sasaki, Microstructure and Mechanical Properties of A7075 Alloy with Additional Si Objects Fabricated by Selective Laser Melting, MATERIALS TRANSACTIONS 60(10) (2019) 2143-2150.
[162] Y. Otani, S. Sasaki, Effects of the addition of silicon to 7075 aluminum alloy on microstructure, mechanical properties, and selective laser melting processability, Materials Science and Engineering: A 777 (2020) 139079.
[163] T. Qi, H. Zhu, H. Zhang, J. Yin, L. Ke, X. Zeng, Selective laser melting of Al7050 powder: Melting mode transition and comparison of the characteristics between the keyhole and conduction mode, Materials & Design 135 (2017) 257-266.
[164] N. Kaufmann, M. Imran, T.M. Wischeropp, C. Emmelmann, S. Siddique, F. Walther, Influence of Process Parameters on the Quality of Aluminium Alloy EN AW 7075 Using Selective Laser Melting (SLM), Physics Procedia 83 (2016) 918-926.
[165] C.M. Gourlay, A.K. Dahle, Dilatant shear bands in solidifying metals, Nature 445(7123) (2007) 70-73.
[166] F.J. Humphreys, P.B. Prangnell, R. Priestner, Fine-grained alloys by thermomechanical processing, Current Opinion in Solid State and Materials Science 5(1) (2001) 15-21.
[167] B.S. Murty, S.A. Kori, M. Chakraborty, Grain refinement of aluminium and its alloys by heterogeneous nucleation and alloying, International Materials Reviews 47(1) (2002) 3-29.
[168] M. Easton, D. StJohn, Grain refinement of aluminum alloys: Part I. the nucleant and solute paradigms—a review of the literature, Metallurgical and Materials Transactions A 30(6) (1999) 1613-1623.
[169] D. Turnbull, B. Vonnegut, Nucleation Catalysis, Industrial & Engineering Chemistry 44(6) (1952) 1292-1298.
[170] A.L. Greer, A.M. Bunn, A. Tronche, P.V. Evans, D.J. Bristow, Modelling of inoculation of metallic melts: application to grain refinement of aluminium by Al–Ti–B, Acta Materialia 48(11) (2000) 2823-2835.
[171] W.C. Winegard, B. Chalmers, Supercooling and dendritic freezing in alloys, Transactions of American Society for Metals 46 (1954) 1214-1224.
[172] D.H. StJohn, M. Qian, M.A. Easton, P. Cao, The Interdependence Theory: The relationship between grain formation and nucleant selection, Acta Materialia 59(12) (2011) 4907-4921.
[173] M.A. Easton, D.H. StJohn, A model of grain refinement incorporating alloy constitution and potency of heterogeneous nucleant particles, Acta Materialia 49(10) (2001) 1867-1878.
[174] X.B. Qi, Y. Chen, X.H. Kang, D.Z. Li, Q. Du, An analytical approach for predicting as-cast grain size of inoculated aluminum alloys, Acta Materialia 99 (2015) 337-346.
[175] Y.K. Xiao, Z.Y. Bian, Y. Wu, G. Ji, Y.Q. Li, M.J. Li, Q. Lian, Z. Chen, A. Addad, H.W. Wang, Effect of nano-TiB2 particles on the anisotropy in an AlSi10Mg alloy processed by selective laser melting, Journal of Alloys and Compounds 798 (2019) 644-655.
[176] G. A.L., C. P.S., M. M.W., S. W., S. P., S. J.A., T. A., Grain Refinement of Aluminium Alloys by Inoculation, Advanced Engineering Materials 5(1-2) (2003) 81-91.
[177] D. Carluccio, M.J. Bermingham, Y. Zhang, D.H. StJohn, K. Yang, P.A. Rometsch, X. Wu, M.S. Dargusch, Grain refinement of laser remelted Al-7Si and 6061 aluminium alloys with Tibor® and scandium additions, Journal of Manufacturing Processes 35 (2018) 715-720.
[178] P. Wang, C. Gammer, F. Brenne, T. Niendorf, J. Eckert, S. Scudino, A heat treatable TiB2/Al-3.5Cu-1.5Mg-1Si composite fabricated by selective laser melting: Microstructure, heat treatment and mechanical properties, Composites Part B: Engineering 147 (2018) 162-168.

[179] X. Wen, Q. Wang, Q. Mu, N. Kang, S. Sui, H. Yang, X. Lin, W. Huang, Laser solid forming additive manufacturing TiB2 reinforced 2024Al composite: Microstructure and mechanical properties, Materials Science and Engineering: A 745 (2019) 319-325.
[180] Q. Tan, Y. Yin, Z. Fan, J. Zhang, Y. Liu, M.-X. Zhang, Uncovering the roles of LaB6-nanoparticle inoculant in the AlSi10Mg alloy fabricated via selective laser melting, Materials Science and Engineering: A 800 (2021) 140365.
[181] Q. Tan, J. Zhang, N. Mo, Z. Fan, Y. Yin, M. Bermingham, Y. Liu, H. Huang, M.-X. Zhang, A novel method to 3D-print fine-grained AlSi10Mg alloy with isotropic properties via inoculation with LaB6 nanoparticles, Additive Manufacturing 32 (2020) 101034.
[182] F. Wang, Z. Liu, D. Qiu, J.A. Taylor, M.A. Easton, M.-X. Zhang, Revisiting the role of peritectics in grain refinement of Al alloys, Acta Materialia 61(1) (2013) 360-370.
[183] X. Nie, H. Zhang, H. Zhu, Z. Hu, L. Ke, X. Zeng, Effect of Zr content on formability, microstructure and mechanical properties of selective laser melted Zr modified Al-4.24Cu-1.97Mg-0.56Mn alloys, Journal of Alloys and Compounds 764 (2018) 977-986.
[184] J. Røyset, N. Ryum, Scandium in aluminium alloys, International Materials Reviews 50(1) (2005) 19-44.
[185] L. Zhou, H. Pan, H. Hyer, S. Park, Y. Bai, B. McWilliams, K. Cho, Y. Sohn, Microstructure and tensile property of a novel AlZnMgScZr alloy additively manufactured by gas atomization and laser powder bed fusion, Scripta Materialia 158 (2019) 24-28.
[186] T. Yuan, S. Kou, Z. Luo, Grain refining by ultrasonic stirring of the weld pool, Acta Materialia 106 (2016) 144-154.
[187] S. Kou, Y. Le, Grain structure and solidification cracking in oscillated arc welds of 5052 aluminum alloy, Metallurgical Transactions A 16(7) (1985) 1345-1352.
[188] Y. Zhang, Y. Guo, Y. Chen, Y. Cao, H. Qi, S. Yang, Microstructure and Mechanical Properties of Al-12Si Alloys Fabricated by Ultrasonic-Assisted Laser Metal Deposition, Materials 13(1) (2020) 126.
[189] C.J. Todaro, M.A. Easton, D. Qiu, D. Zhang, M.J. Bermingham, E.W. Lui, M. Brandt, D.H. StJohn, M. Qian, Grain structure control during metal 3D printing by high-intensity ultrasound, Nature Communications 11(1) (2020) 142.
[190] M. Gremaud, D.R. Allen, M. Rappaz, J.H. Perepezko, The development of nucleation controlled microstructures during laser treatment of AlSi alloys, Acta Materialia 44(7) (1996) 2669-2681.
[191] J.H. Tan, W.L.E. Wong, K.W. Dalgarno, An overview of powder granulometry on feedstock and part performance in the selective laser melting process, Additive Manufacturing 18 (2017) 228-255.
[192] H.H. Zhu, J.Y.H. Fuh, L. Lu, The influence of powder apparent density on the density in direct laser-sintered metallic parts, International Journal of Machine Tools and Manufacture 47(2) (2007) 294-298.
[193] A.B. Spierings, M. Voegtlin, T. Bauer, K. Wegener, Powder flowability characterisation methodology for powder-bed-based metal additive manufacturing, Progress in Additive Manufacturing 1(1) (2016) 9-20.
[194] A. Popovich, V. Sufiiarov, Metal Powder Additive Manufacturing, New Trends 3D Print (2016).
[195] S. Vock, B. Klöden, A. Kirchner, T. Weißgärber, B. Kieback, Powders for powder bed fusion: a review, Progress in Additive Manufacturing 4(4) (2019) 383-397.
[196] R.J. Hebert, Viewpoint: metallurgical aspects of powder bed metal additive manufacturing, Journal of Materials Science 51(3) (2016) 1165-1175.
[197] C.C. Furnas, Grading Aggregates - I. - Mathematical Relations for Beds of Broken Solids of Maximum Density, Industrial & Engineering Chemistry 23(9) (1931) 1052-1058.
[198] A.E.R. Westman, THE PACKING OF PARTICLES: EMPIRICAL EQUATIONS FOR INTERMEDIATE DIAMETER RATIOS*, Journal of the American Ceramic Society 19(1-12) (1936) 127-129.
[199] R.K. McGEARY, Mechanical Packing of Spherical Particles, Journal of the American Ceramic Society 44(10) (1961) 513-522.
[200] E. Olatunde Olakanmi, W. Dalgarno Kenneth, F. Cochrane Robert, Laser sintering of blended Al-Si powders, Rapid Prototyping Journal 18(2) (2012) 109-119.

[201] J.A. Muñiz-Lerma, A. Nommeots-Nomm, K.E. Waters, M. Brochu, A Comprehensive Approach to Powder Feedstock Characterization for Powder Bed Fusion Additive Manufacturing: A Case Study on AlSi7Mg, Materials (Basel) 11(12) (2018).
[202] A. Strondl, O. Lyckfeldt, H. Brodin, U. Ackelid, Characterization and Control of Powder Properties for Additive Manufacturing, JOM 67(3) (2015) 549-554.
[203] J.A. Slotwinski, E.J. Garboczi, P.E. Stutzman, C.F. Ferraris, S.S. Watson, M.A. Peltz, Characterization of Metal Powders Used for Additive Manufacturing, J Res Natl Inst Stand Technol 119 (2014) 460-493.
[204] L.J. Jallo, M. Schoenitz, E.L. Dreizin, R.N. Dave, C.E. Johnson, The effect of surface modification of aluminum powder on its flowability, combustion and reactivity, Powder Technology 204(1) (2010) 63-70.
[205] Front Matter, Fundamentals of Refractory Technology2006, pp. i-vii.
[206] A. Hodgson, S. Haq, Water adsorption and the wetting of metal surfaces, Surface Science Reports 64(9) (2009) 381-451.
[207] J.M. Oh, B.G. Lee, S.W. Cho, S.W. Lee, G.S. Choi, J.W. Lim, Oxygen effects on the mechanical properties and lattice strain of Ti and Ti-6Al-4V, Metals and Materials International 17(5) (2011) 733-736.
[208] Z. Hu, H. Zhu, X. Nie, C. Zhang, H. Zhang, X. Zeng, On the role of atmospheric oxygen into mechanical properties and fracture behavior of selective laser melted AlCu5MnCdVA, Materials & Design 150 (2018) 18-27.
[209] V. Karde, C. Ghoroi, Fine powder flow under humid environmental conditions from the perspective of surface energy, International Journal of Pharmaceutics 485(1) (2015) 192-201.